# *Ab initio* construction of symmetry-adapted k · p Hamiltonians for the electronic structure of semiconductors

Milan Jocić[*] and Nenad Vukmirović [†]

*Institute of Physics Belgrade, University of Belgrade, Pregrevica 118, 11080 Belgrade, Serbia*

While **k · p** Hamiltonians are frequently used for the description of electronic states in quantum nanostructures, a method is lacking to obtain them in their symmetrized form directly from *ab initio* band structure calculations of bulk material. We developed a method for obtaining the parameters and the symmetry-adapted form of the **k · p** Hamiltonian from the output of an *ab initio* band structure calculation. The method consists of (i) evaluation of momentum matrix elements between the wave functions obtained from band structure calculation; (ii) identification of the unitary transformation that transforms these wave functions to the symmetry-adapted basis; (iii) transformation of the **k · p** Hamiltonian to the symmetry-adapted basis. We illustrate the methodology by obtaining **k · p** Hamiltonians that describe the band structure of zinc-blende CdSe and then we use the Hamiltonians obtained to calculate the electronic states in CdSe quantum wells. Excellent agreement between density functional theory and **k · p** is obtained for the electronic structure, even for quite thin wells.

## I. INTRODUCTION

Semiconductor materials and nanostructures based upon them are at the heart of the operation of almost all electronic and optical devices. For this reason, there is a significant interest in understanding the electronic states in these materials. The progress in developments of methodologies for *ab initio* electronic structure calculations has led us to the point where it is relatively straightforward to perform band structure calculations of bulk semiconducting materials. Density functional theory (DFT) calculations based on local or semilocal approximations for the exchange-correlation functional give band gaps that are significantly smaller than experimental band gaps [1]. However, improved treatments based on the use of hybrid functionals [2,3] or many body perturbation theory in GW (where G stands for the Green's function and W for screened Coulomb interaction) approximation [4] give rather accurate band gaps and band structure of the bulk material [5–7]. On the other hand, it is rather difficult to perform *ab initio* calculations of semiconductor nanostructures because the calculation needs to be performed for a supercell containing a very large number of atoms.

The method that proved to be both practical and successful in treating the electronic states in semiconductor nanostructures is the **k · p** method [8–11]. It is based on the representation of the single-particle wave function in terms of Bloch functions of the bulk material at a certain point in the Brillouin zone (typically the Γ point) and slowly varying envelope functions. The **k · p** Hamiltonian for a nanostructure is then an operator that acts on the column of envelope functions corresponding to each of the bulk bands.

Despite the success in using the **k · p** method for description of bulk band structure around a certain point in the Brillouin zone (usually the Γ point) and for treating the semiconductor nanostructures, there is still no systematic way to construct the **k · p** Hamiltonian for a given material and obtain the parameters of the Hamiltonian. The parameters of most conventional **k · p** Hamiltonians (such as the eight-band Hamiltonian [10,12,13]) for a few most common classes of semiconductors can be found in the literature [14,15] and were obtained from the band gap and effective masses in the valence and conduction band. Parameters of **k · p** Hamiltonians with larger number of bands (such as, for example, the 30-band Hamiltonian [16–20]) and recently introduced atomistic **k · p** [21] are typically obtained by fitting to the calculated band structure of the material or to experimental data. However, given a relatively large number of fitting parameters, it is questionable if the fit gives unique parameters. It is also not clear what part of the Brillouin zone should be used in the fitting procedure, since it is not expected that the **k · p** method describes the bulk band structure throughout the whole Brillouin zone.

Given the fact that new classes of semiconductor materials and nanostructures based upon them emerge or find new applications quite often, it would be of significant interest to develop the procedure for construction of desired **k · p** Hamiltonians. Since all parameters of the **k · p** Hamiltonian are related to momentum matrix elements between single-particle wave functions of the bulk, it is in principle possible to obtain them from electronic structure calculation of the bulk material. This is indeed done when **k · p** is used as a method for interpolation of *ab initio* calculated band structure to a more dense grid of **k** points [22–25]. However, there is a certain shortcoming of this approach when it comes to the construction of **k · p** Hamiltonians that should be used in future applications. Namely, due to the symmetry of the

---

*milan.jocic@ipb.ac.rs
†nenad.vukmirovic@ipb.ac.rs

085121-1

crystalline material the energy levels in characteristic points in the Brillouin zone are degenerate and for this reason the choice of Bloch wave functions from the Hilbert space spanned by the degenerate states is not unique. As a consequence, one may end up with different forms of the final $\mathbf{k} \cdot \mathbf{p}$ Hamiltonian depending on the particular choice of Bloch functions from this space. The number of Hamiltonian parameters in these forms might be significantly larger than the true number of parameters imposed by the symmetry of the crystal.

In this work, we develop the procedure for construction of the $\mathbf{k} \cdot \mathbf{p}$ Hamiltonian in the symmetrized form with a minimal number of parameters imposed by crystal symmetry. In Sec. II we give a brief overview of the $\mathbf{k} \cdot \mathbf{p}$ method and present our approach for the construction of the Hamiltonian. In Sec. III we illustrate the method by applying it to bulk zinc-blende CdSe and to CdSe quantum wells.

## II. THEORETICAL APPROACH

### A. $\mathbf{k} \cdot \mathbf{p}$ equation

We start this section by briefly reviewing the $\mathbf{k} \cdot \mathbf{p}$ method to set the stage for description of our procedure for construction of $\mathbf{k} \cdot \mathbf{p}$ Hamiltonian. We start with the equation for an electron in the periodic crystal that reads

$$\left[ \frac{p^2}{2m_0} + U + T_{\mathrm{rk}} + H_{\mathrm{D}} + H_{\mathrm{soc}} \right] |\Psi_{n\mathbf{k}}\rangle = E_n(\mathbf{k})|\Psi_{n\mathbf{k}}\rangle, \quad (1)$$

where $p^2/(2m_0) = -\hbar^2 \nabla^2/(2m_0)$ is the kinetic energy operator and $m_0$ is the free electron mass, $U$ is the periodic crystal potential (including nuclei, core and valence electrons), while $E_n(\mathbf{k})$ and $|\Psi_{n\mathbf{k}}\rangle$ are the corresponding energy and wave function for the electron in band $n$ at wave vector $\mathbf{k}$ in the Brillouin zone. When the effects of spin-orbit interaction are included, $|\Psi_{n\mathbf{k}}\rangle$ is a two-component spinor. The last three terms in brackets are the relativistic corrections accounting for kinetic energy $T_{\mathrm{rk}} = -p^4/(8m_0^3 c^2)$, fine structure through the Darwin term $H_{\mathrm{D}} = \hbar^2 \nabla \cdot \nabla U/(8m_0^2 c^2)$ and spin-orbit coupling (SOC) $H_{\mathrm{soc}} = \hbar(\sigma \times \nabla U) \cdot \mathbf{p}/(4m_0^2 c^2)$, where $\sigma = (\sigma_x, \sigma_y, \sigma_z)$ denotes a vector with Pauli matrices as its components.

For an electron in a periodic potential, the Bloch theorem holds, by which the components of $|\Psi_{n\mathbf{k}}\rangle$ are of the form

$$\Psi_{n\mathbf{k}}^{(a)}(\mathbf{r}) = e^{i\mathbf{k} \cdot \mathbf{r}} u_{n\mathbf{k}}^{(a)}(\mathbf{r}), \quad (2)$$

where $u_{n\mathbf{k}}^{(a)}(\mathbf{r})$ are periodic Bloch functions satisfying the condition $u_{n\mathbf{k}}^{(a)}(\mathbf{r} + \mathbf{R}) = u_{n\mathbf{k}}^{(a)}(\mathbf{r})$, with $\mathbf{R}$ being the direct lattice vector. Inserting Eq. (2) into Eq. (1), we obtain the one-electron equation in terms of periodic Bloch functions:

$$\left[ H + \frac{\hbar^2 k^2}{2m_0} + T_{\mathrm{rk}}'(\mathbf{k}) + \frac{\hbar \mathbf{k} \cdot \mathbf{p}_{\mathrm{soc}}}{m_0} \right] |u_{n\mathbf{k}}\rangle = E_n(\mathbf{k})|u_{n\mathbf{k}}\rangle, \quad (3)$$

where $H = p^2/(2m_0) + U + T_{\mathrm{rk}} + H_{\mathrm{D}} + H_{\mathrm{soc}}$ is the initial Hamiltonian from Eq. (1), $\mathbf{p}_{\mathrm{soc}} = \mathbf{p} + \hbar(\sigma \times \nabla U)/(4m_0 c^2)$ is the momentum modified with the SOC part and $T_{\mathrm{rk}}'(\mathbf{k})$ is given as

$$T_{\mathrm{rk}}'(\mathbf{k}) = -\frac{1}{8m_0^3 c^2}[4(\hbar\mathbf{k} \cdot \mathbf{p})p^2 + 4(\hbar\mathbf{k} \cdot \mathbf{p})^2$$
$$+ 4(\hbar k)^2(\hbar\mathbf{k} \cdot \mathbf{p}) + 2(\hbar k)^2 p^2 + (\hbar k)^4]. \quad (4)$$

We further express $|u_{a\mathbf{k}}\rangle$ in the basis of orthonormal functions $|u_{m\mathbf{k}_0}\rangle$:

$$|u_{a\mathbf{k}}\rangle = \sum_m B_m^{(a)}(\mathbf{k})|u_{m\mathbf{k}_0}\rangle, \quad (5)$$

which are solutions of eigenproblem given by Eq. (3) at a certain $\mathbf{k}_0$ with eigenvalues $E_n(\mathbf{k}_0)$. Inserting Eq. (5) into Eq. (3), multiplying from the left by $\langle u_{n\mathbf{k}_0}|$ and exploiting the orthonormality condition we arrive at the equation

$$\sum_m \left[ \left( E_n(\mathbf{k}_0) + \frac{\hbar^2(k^2 - k_0^2)}{2m_0} \right) \delta_{nm} \right.$$
$$\left. + \frac{\hbar(\mathbf{k} - \mathbf{k}_0)}{m_0} \cdot \langle u_{n\mathbf{k}_0}|\mathbf{p}|u_{m\mathbf{k}_0}\rangle \right] B_m^{(a)}(\mathbf{k})$$
$$= E^{(a)}(\mathbf{k})B_n^{(a)}(\mathbf{k}). \quad (6)$$

We have omitted $T_{\mathrm{rk}}'(\mathbf{k}, \mathbf{k}_0)$ that would appear in Eq. (6) because its contribution depends directly on the distance between $\mathbf{k}$ and $\mathbf{k}_0$ and becomes significant at distances far greater than the one where $\mathbf{k} \cdot \mathbf{p}$ theory is applicable. We have performed a numerical check of this claim in case of zinc-blende CdSe and we have shown that the influence of this term on bulk eigenenergies is smaller than 0.3 meV throughout the whole Brillouin zone. For similar reasons, we neglected SOC modification to momentum (i.e., we take $\mathbf{p}_{\mathrm{soc}} \approx \mathbf{p}$). We note that SOC is fully included in our approach unlike in many theoretical treatments where it is treated as a perturbation. We further rewrite Eq. (6) in somewhat more convenient form by exploiting the relation

$$\langle \Psi_{n\mathbf{k}_0}|\mathbf{p}|\Psi_{m\mathbf{k}_0}\rangle = \hbar\mathbf{k}\delta_{nm} + \langle u_{n\mathbf{k}_0}|\mathbf{p}|u_{m\mathbf{k}_0}\rangle. \quad (7)$$

We then obtain

$$\sum_m \left[ \left( E_n(\mathbf{k}_0) + \frac{\hbar^2(\mathbf{k} - \mathbf{k}_0)^2}{2m_0} \right) \delta_{nm} \right.$$
$$\left. + \frac{\hbar(\mathbf{k} - \mathbf{k}_0)}{m_0} \cdot \langle \Psi_{n\mathbf{k}_0}|\mathbf{p}|\Psi_{m\mathbf{k}_0}\rangle \right] B_m^{(a)}(\mathbf{k})$$
$$= E^{(a)}(\mathbf{k})B_n^{(a)}(\mathbf{k}), \quad (8)$$

which takes the form of an eigenproblem:

$$\sum_m H_{nm}^{(1)} B_m^{(a)} = E^{(a)} B_n^{(a)}, \quad (9)$$

where $H_{nm}^{(1)}$ is given by the term in square brackets in Eq. (8). The indices $m$ and $n$ in Eq. (9) go over the bands that were included in the expansion in Eq. (5). The accuracy of $\mathbf{k} \cdot \mathbf{p}$ Hamiltonian can further be improved by adding the effect of remote bands [the bands not included in the expansion in Eq. (5)] perturbatively using the Löwdin's perturbation theory [11,26]. This yields additional term in the $\mathbf{k} \cdot \mathbf{p}$ Hamiltonian which reads

$$H_{nm}^{(2)} = \frac{\hbar^2}{m_0^2} \sum_l \frac{\langle u_{n\mathbf{k}_0}|\mathbf{K} \cdot \mathbf{p}|u_{l\mathbf{k}_0}\rangle \langle u_{l\mathbf{k}_0}|\mathbf{K} \cdot \mathbf{p}|u_{m\mathbf{k}_0}\rangle}{[E_n(\mathbf{k}_0) + E_m(\mathbf{k}_0)]/2 - E_l(\mathbf{k}_0)}, \quad (10)$$

with $\mathbf{K} = \mathbf{k} - \mathbf{k}_0$ and the summation goes over the bands $l$ that were not included in the expansion in Eq. (5).

### B. Construction of symmetrized k · p Hamiltonian

The expression (8) can be, in principle, used to construct the **k** · **p** Hamiltonian directly from *ab initio* calculation of band structure of bulk. Namely, all Hamiltonian matrix elements can be calculated from band energies $E_n(\mathbf{k}_0)$ at point $\mathbf{k}_0$ and momentum matrix elements $\langle \Psi_{n\mathbf{k}_0}|\mathbf{p}|\Psi_{m\mathbf{k}_0}\rangle$ between the wave functions at $\mathbf{k}_0$. However, an issue arises regarding the uniqueness of the constructed Hamiltonian matrix as a consequence of the fact that some of the eigenstates $|\Psi_{n\mathbf{k}_0}\rangle$ are degenerate. A typical choice for the $\mathbf{k}_0$ point is some high symmetry point where band dispersions exhibit minima or maxima (such as for example the $\Gamma$ point) and the group $G_{\mathbf{k}_0}$ of the wave vector $\mathbf{k}_0$ is some high symmetry point group. For this reason, there is a degeneracy between the eigenstates at $\mathbf{k}_0$, where the degree of degeneracy is determined by the dimensions of irreducible representations (irreps) of the group $G_{\mathbf{k}_0}$ corresponding to each of the states. For example, in the case of zinc-blende CdSe material used as an example in this work, the top valence band is threefold degenerate and the bottom conduction band is nondegenerate when spin degrees of freedom are not taken into account and the effect of spin-orbit interaction is not included. When spin-orbit interaction is included, the bottom conduction band is twofold degenerate, while two top valence bands are twofold and fourfold degenerate.

Let $d$ be the degeneracy of the set of eigenstates $|\phi_1\rangle, |\phi_2\rangle, \ldots, |\phi_d\rangle$ at $\mathbf{k}_0$ at let $\mathcal{H}_d$ be the Hilbert space spanned by these states. The states $|\phi_1\rangle, |\phi_2\rangle, \ldots, |\phi_d\rangle$ form an orthonormal basis of $\mathcal{H}_d$ but any other orthonormal basis may well have been chosen. With the use of different basis, the momentum matrix elements in Eq. (8) would be different and the **k** · **p** Hamiltonian would have a different form. Moreover, it might even appear that the Hamiltonian has a different number of parameters. Our goal is to overcome this issue by fixing the choice of the degenerate states and obtaining the **k** · **p** Hamiltonian in the form where it has a minimal number of parameters imposed by the symmetry group $G_{\mathbf{k}_0}$ of the wave vector $\mathbf{k}_0$.

The set $|\phi_1\rangle, |\phi_2\rangle, \ldots, |\phi_d\rangle$ is obtained from DFT and they form $d \times d$ matrices $\Gamma(g)$ of the irrep of group $G_{\mathbf{k}_0}$ that are given as

$$\Gamma_{mn}(g) = \langle \phi_m | P(g) | \phi_n \rangle, \tag{11}$$

where $g$ is an element of the group $G_{\mathbf{k}_0}$ and $P(g)$ is the operator that applies the symmetry operation $g$ on the given wave function. The matrices $\Gamma(g)$ are then obtained by directly calculating the matrix elements in Eq. (11). We then calculate the characters of $\Gamma$ to match it with one of the equivalent conventional irreps $\Gamma'$ of the point group $G_{\mathbf{k}_0}$. The matrices of irreps $\Gamma'$ can be found in databases of irreps of point groups, for example in Bilbao crystallographic data server [27]. The matrices $\Gamma(g)$ and $\Gamma'(g)$ are connected via a unitary transformation

$$U^\dagger \Gamma(g) U = \Gamma'(g), \tag{12}$$

which is satisfied for each $g \in G_{\mathbf{k}_0}$. Therefore, to obtain the basis of states in $\mathcal{H}_d$ which is adapted to conventional matrices $\Gamma'(g)$ in databases of irreps, one has to make a unitary

transformation of the basis

$$|\psi_j\rangle = \sum_{i=1}^{d} U_{ij} |\phi_i\rangle. \tag{13}$$

Now, the representation of the operator $P(g)$ from Eq. (11) in the new basis set $|\psi_j\rangle$ is the conventional representation $\Gamma'$. In the $|\psi_j\rangle$ basis, the **k** · **p** Hamiltonian has a convenient, symmetry-adapted form, in which relevant parameters of the Hamiltonian can be straightforwardly identified.

It remains to define a procedure for obtaining the unitary matrix $U$ that connects the two representations $\Gamma$ and $\Gamma'$. Such a procedure has recently been developed in Ref. [28] and we outline it here. One first obtains a set of coefficients $r_{ab}$ as

$$r_{ab} = \sqrt{\frac{n_\Gamma}{|G|}} \left( \sum_{g \in G} \Gamma_{aa}(g) \Gamma'_{bb}(g^{-1}) \right)^{1/2}, \tag{14}$$

where $\Gamma_{aa}(g)$ and $\Gamma'_{bb}(g^{-1})$ are known matrix elements for symmetry operation (group element) $g$ and its inverse $g^{-1}$, respectively, $|G|$ is the order of group $G$ while $n_\Gamma$ is the dimension of representations $\Gamma$ and $\Gamma'$. Then, one chooses the pair $(a, b)$ for which $r_{ab} > 0$. The existence of such a pair has been proven in Ref. [28]. The matrix $U$ is then given as

$$U_{ij} = \frac{1}{r_{ab}} \frac{n_\Gamma}{|G|} \sum_{g \in G} \Gamma_{ia}(g^{-1}) \Gamma'_{bj}(g). \tag{15}$$

With this, we complete our procedure for construction of symmetrized **k** · **p** Hamiltonian. For clarity, we review all steps of the procedure here:

(i) Perform *ab initio* calculation of band structure for bulk, using DFT with local functionals, hybrid functional DFT, or by including quasiparticle energy correction within the GW approximation.

(ii) Choose the point $\mathbf{k}_0$ in the Brillouin zone, that is most suited for **k** · **p** expansion and extract band energies $E_n(\mathbf{k}_0)$ and their eigenstates $|\Psi_{n\mathbf{k}_0}\rangle$ from desired *ab initio* method.

(iii) Identify the groups of degenerate states at $\mathbf{k}_0$ and the symmetry point group $G_{\mathbf{k}_0}$. Select the groups of degenerate states (usually those around the gap) that will form the **k** · **p** Hamiltonian. Extract these groups of degenerate states $|\phi_i\rangle$ from *ab initio* eigenstates $|\Psi_{n\mathbf{k}_0}\rangle$.

(iv) For each of selected groups of degenerate states calculate the matrices $\Gamma(g)$ of corresponding irrep $\Gamma$ using Eq. (11). Using characters of $\Gamma(g)$, match $\Gamma$ to the equivalent conventional representation $\Gamma'$ found in databases of irreps of point groups.

(v) For each of selected groups of degenerate states, calculate the unitary matrices $U$ using sets of matrices $\Gamma(g)$ and $\Gamma'(g)$ as inputs for Eqs. (14) and (15).

(vi) Proceed with calculation of the new, symmetry-adapted basis, consisting of selected groups of degenerate states $|\psi_j\rangle$ using matrices $U$, obtained from the previous step, and corresponding groups of degenerate states $|\phi_i\rangle$ with Eq. (13).

(vii) Evaluate the momentum matrix elements in the new basis using Eqs. (7) (8), (9), and (10) which then

give all parameters of the symmetrized $\mathbf{k} \cdot \mathbf{p}$ Hamiltonian $H_{nm} = H_{nm}^{(1)} + H_{nm}^{(2)}$.

It is important to note that these steps constitute a well-defined and straightforward procedure that gives the desired $\mathbf{k} \cdot \mathbf{p}$ Hamiltonian starting from output of an *ab initio* calculation. It does not involve any kind of fitting which would introduce certain arbitrariness.

Next, we discuss the form of the Hamiltonian that we obtain and its relation to the form of the Hamiltonian that would be obtained using Luttinger's method of invariants [11,29]. The form of the Hamiltonian that we obtain consists of blocks $\mathcal{B}(\Gamma'_a, \Gamma'_b)$, where each block originates from two groups of states: the states $|\psi_1^{(a)}\rangle, \ldots, |\psi_{d_a}^{(a)}\rangle$ that transform in accordance with the representation $\Gamma'_a$ of dimension $d_a$ and the states $|\psi_1^{(b)}\rangle, \ldots, |\psi_{d_b}^{(b)}\rangle$ that transform in accordance with the representation $\Gamma'_b$ of dimension $d_b$. The Hamiltonian consists of the terms quadratic in electronic momentum $K$, the terms linear in $K$ and the terms that do not contain $K$. Luttinger's method of invariants [11,29] gives a systematic way to obtain the form of each $\mathcal{B}(\Gamma'_a, \Gamma'_b)$ for terms of given order in $K$. For this reason, our procedure yields the same form of the Hamiltonian as Luttinger's method of invariants applied to obtain the terms up to second order in $K$. By its construction, Luttinger's method fully exploits the point group symmetry and yields the Hamiltonian in the form where a minimal number of parameters appears. On the other hand, it is clear that Luttinger's method cannot give the values of these parameters, since it exploits the symmetry of the system only and does not consider other details of the system. Our procedure in some sense links Luttinger's method from 1950's to modern *ab initio* calculations as it enables to obtain the form of the Hamiltonian that would be obtained using Luttinger's method and additionally gives the values of these parameters starting from *ab initio* wave functions and energies.

In Sec. III we apply our procedure to zinc-blende CdSe crystal whose point group at the $\Gamma$ point is the $T_d$ group. However, we note that our procedure is by no means limited to this particular crystal symmetry. It can be used for crystals of any kind of symmetry, at any point $\mathbf{k}_0$ in the Brillouin zone. Of course, benefits of this method will be greater if the symmetry point group $G_{\mathbf{k}_0}$ at $\mathbf{k}_0$ is of higher order. Having a symmetry-adapted form of the Hamiltonian also gives great advantage when it comes to calculation of nanostructures. Numerical codes for calculating nanostructures using $\mathbf{k} \cdot \mathbf{p}$ Hamiltonians could be easily adapted to another material of the same symmetry by just changing the numerical values of the parameters, that can be straightforwardly obtained using *ab initio* calculation for bulk material and the procedure described in the paper.

Finally, we briefly discuss on the conventions for matrices of the representations $\Gamma'$. In all examples in this work we have taken the matrices from Bilbao crystallographic data server [27] and consequently we used the conventions used therein. Unfortunately, this is not the only convention in the literature. The discussion on the effect of the choice of the convention for $\Gamma'$ on the form of basis states $|\psi_i\rangle$ and the form of $\mathbf{k} \cdot \mathbf{p}$ Hamiltonian is given at the end of Secs. II B and II C of Ref. [30].

## III. RESULTS

In this section, we apply the methodology described in Sec. II to bulk zinc-blende CdSe crystal and to zinc-blende CdSe quantum well. We apply the methodology to obtain the form and the parameters of the $8 \times 8$ ($4 \times 4$) and $26 \times 26$ ($13 \times 13$) symmetry adapted $\mathbf{k} \cdot \mathbf{p}$ Hamiltonian with (without) spin-orbit interaction included for CdSe in the zinc-blende structure. We will refer to the $8 \times 8$ ($4 \times 4$) Hamiltonian as the standard Hamiltonian, while $26 \times 26$ ($13 \times 13$) Hamiltonian will be referred to as the extended Hamiltonian.

The band energies and wave functions were obtained from DFT where exchange-correlation energy was modeled using the Perdew-Burke-Ernzerhof generalized gradient approximation revised for solids (PBEsol) [31]. Calculations were performed using the Quantum Espresso code [32,33]. Core electrons were modeled using fully relativistic optimized normconserving Vanderbilt pseudopotentials [34,35]. The $10 \times 10 \times 10$ grid in reciprocal space of the Brillouin zone was used, while the kinetic energy cutoff of the plane waves used to represent the wave functions was 90 Ry. The lattice constant of $a = 6.096$ Å, obtained by minimization of the energy of the structure, was used in all subsequent calculations.

Since local and semilocal approximations in DFT do not give accurate values of the band gap [1], we have also performed the band structure calculation using many-body perturbation theory in the GW approximation [4]. Within this approach, the electron self-energy is approximated using the expression containing the Green's function G and the screened Coulomb interaction W. In this work, we used the $G_0W_0$ variant of GW approximation in which the self-energy is obtained from Green's function $G_0$ of an electron in DFT Kohn-Sham potential, without further iterations. The calculations were performed using the YAMBO code [36,37], with input Kohn-Sham wave functions obtained from a previous DFT calculation on the $4 \times 4 \times 4$ grid in reciprocal space. Plasmon-pole approximation was used to account for the frequency dependence of the dielectric function. Kinetic energy cutoff used for the calculation of dielectric function in $G_0W_0$ calculation was 50 Ry. The corresponding number of bands was 400 (800), while the number of bands used in the evaluation of self-energy was 300 (600) in the case when spin-orbit interaction is omitted (included). We estimate that these values yield numerical accuracy of 20 meV or better for band energy corrections.

### A. Bulk zinc-blende CdSe

We used the procedure described in Sec. II to obtain the standard and extended $\mathbf{k} \cdot \mathbf{p}$ Hamiltonian in symmetry-adapted form. $\Gamma$ point was chosen as the point $\mathbf{k}_0$ in our procedure, since zinc-blende CdSe exhibits a direct gap at the $\Gamma$ point. The corresponding group $G_{\mathbf{k}_0}$ is then the point symmetry group of the crystal, which is the $T_d$ group in the case of zinc-blende structures. We will denote irreps of this group using the convention of Ref. [38].

We will refer to the states that are included in the standard $\mathbf{k} \cdot \mathbf{p}$ Hamiltonian as the main states, while remaining states included in the extended Hamiltonian will be referred to as
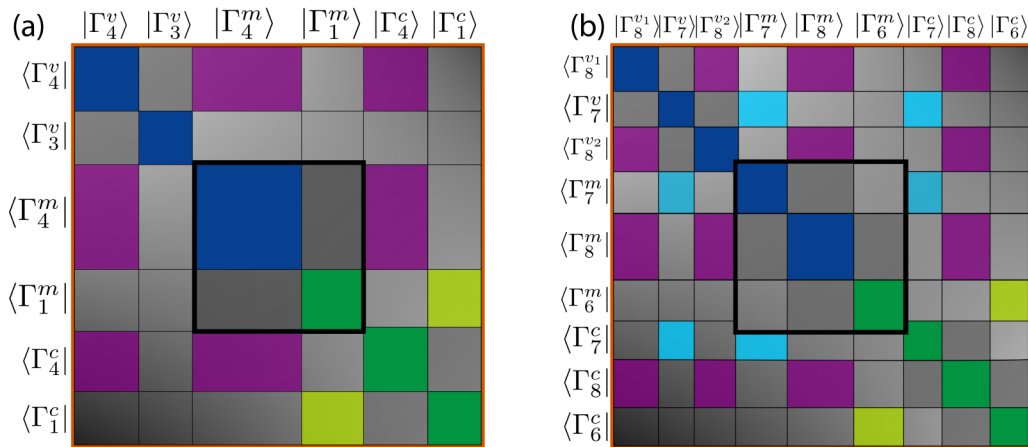
FIG. 1. The form of $\mathbf{k} \cdot \mathbf{p}$ Hamiltonian obtained when spin-orbit interaction is (a) omitted; (b) included. Each block of the matrix contains the terms that originate from matrix elements between the states that transform according to irrep specified on the left and above the matrix. The superscripts $v$, $m$, and $c$ denote the lower valence band states, the main states, and the higher conduction band states. The central square marked with thick black lines denotes the standard Hamiltonian.

lower valence band and higher conduction band states. When spin-orbit interaction is omitted, main states used to construct the standard Hamiltonian are the threefold degenerate $\Gamma_4$ and nondegenerate $\Gamma_1$ states that lie below and above the gap, respectively, giving a total of four states. Extended Hamiltonian is constructed by adding the twofold degenerate $\Gamma_3$ and threefold degenerate $\Gamma_4$ valence states and $\Gamma_4$ and $\Gamma_1$ conduction states, yielding a total of 13 states. When spin-orbit interaction is included, the states transform according to irreps of the double $T_d$ group. The states corresponding to $\Gamma_4$ will split into fourfold $\Gamma_8$ and twofold degenerate $\Gamma_7$ state, the states corresponding to $\Gamma_3$ become fourfold degenerate $\Gamma_8$ and the states corresponding to $\Gamma_1$ become twofold degenerate $\Gamma_6$ states. The characters of the irreps of the single and the double point group $T_d$ are given in Sec. I of Ref. [30].

In Fig. 1, we show the form of both extended and standard Hamiltonian, in cases when the effects of spin-orbit interaction are omitted and included. The Hamiltonian is divided into blocks, where each block originates from two groups of degenerate states with the corresponding irrep shown on the left and above the matrix. These blocks can be absolutely diagonal (connecting same irreps from same states), irrep-diagonal (connecting same irreps from different states) and off-diagonal. When our procedure is applied, each block is obtained in the form with smallest number of parameters in the block, determined by the point group of the crystal. Analytical expressions for the elements of all blocks of the $\mathbf{k} \cdot \mathbf{p}$ Hamiltonian are given in Sec. II of Ref. [30]. We have checked that the same form of the blocks of the Hamiltonian is obtained when Luttinger's method of invariants [11,29] is applied. Numerical values of each parameter appearing in the blocks of the Hamiltonian are given in Sec. III of Ref. [30]. We note that the standard four-band Hamiltonian that we obtain coincides with the second-order four-band Kane Hamiltonian [11]. The standard eight-band Hamiltonian that we obtain coincides with Weiler eight-band Hamiltonian [11,12] after an appropriate unitary transformation is made. The details of this unitary transformation are given in Sec. II B of Ref. [30].

To better illustrate the advantage of using a symmetry-adapted form of the $\mathbf{k} \cdot \mathbf{p}$ Hamiltonian (that is obtained from symmetrized wave functions $|\psi_i\rangle$) rather than the form of the $\mathbf{k} \cdot \mathbf{p}$ Hamiltonian that would be obtained directly from DFT wave functions $|\phi_i\rangle$, we compare the number of parameters in the two forms of the Hamiltonian. The two forms of the four-band Hamiltonian are presented in Sec. II C of Ref. [30]. The number of parameters of the symmetrized form is significantly smaller (1 versus 9 parameters for the terms linear in $k$ and 5 versus 46 parameters for the terms quadratic in $k$), which clearly shows its advantage in terms of simplicity for further use in the study of nanostructures.

In Fig. 2 we plot the band structure of zinc-blende CdSe obtained from DFT calculation and by diagonalizing the standard and extended $\mathbf{k} \cdot \mathbf{p}$ Hamiltonian in cases with and without the effects of spin-orbit interaction. As expected, extended Hamiltonian gives results that are qualitatively and quantitatively closer to full DFT than the standard one. It should be noted that it is preferable to add the states in extended Hamiltonian symmetrically around the main states. We found that expanding the standard Hamiltonian by a noneven number of valence and conduction states can lead to closing of the gap at points far away from $\Gamma$ point. This was more prone to happen if the number of conduction states added was greater than number of valence states added. The presence of such spurious states then prevents the application of the $\mathbf{k} \cdot \mathbf{p}$ Hamiltonian to the nanostructure. Our choice of 13 (26) bands used to construct the extended Hamiltonian was therefore a compromise between (i) the goal to accurately describe the band structure within the part of the Brillouin zone which is as large as possible; (ii) the desire to use the number of bands (and therefore the number of parameters of the $\mathbf{k} \cdot \mathbf{p}$ Hamiltonian) that is not extremely large; (iii) the aim to avoid the appearance of spurious states that close the gap. To quantify in more detail the ability of derived $\mathbf{k} \cdot \mathbf{p}$ Hamiltonians to reproduce the *ab initio* calculated band structure, we plot in Fig. 3 the maximal difference between $\mathbf{k} \cdot \mathbf{p}$ and DFT results within the sphere of radius $k_r$ (which is centered at the $\Gamma$ point) for main bands. We find that standard
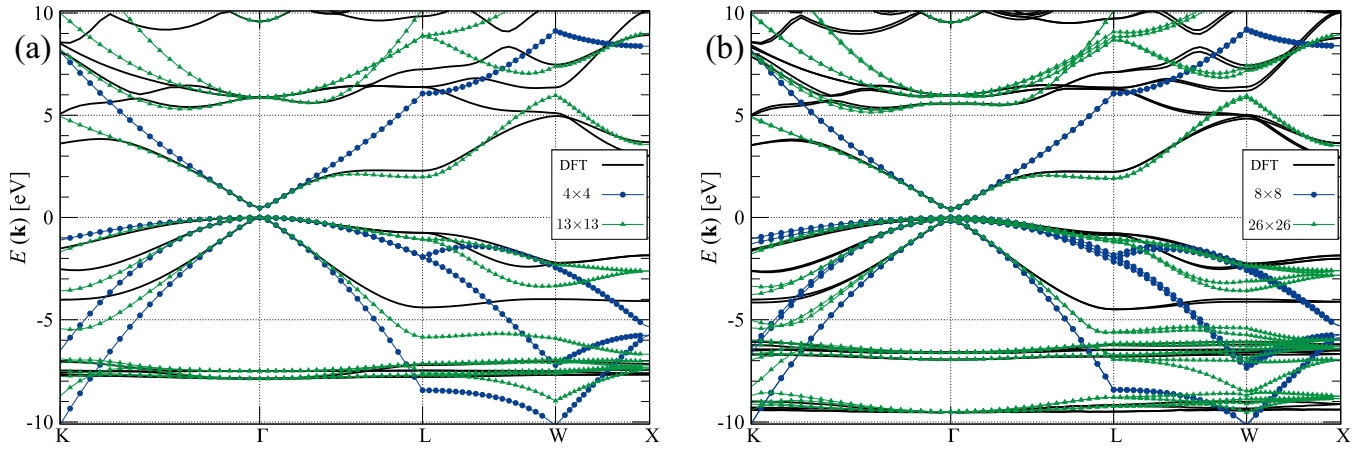
FIG. 2. Band structure of zinc-blende CdSe calculated using DFT and using standard and extended $\mathbf{k} \cdot \mathbf{p}$ Hamiltonian when the effects of spin-orbit interaction are (a) omitted; (b) included.

(extended) $\mathbf{k} \cdot \mathbf{p}$ results differ no more than 4 eV (1.75 eV) inside the sphere inscribed in the first Brillouin zone, with a difference not greater than 45 meV (35 meV) inside a sphere of radius $k_r = 0.2$ in units of $2\pi/a$, where $a$ is the lattice constant. Figure 3 shows that in the reasonable vicinity of $\Gamma$ point, in any direction, extended $\mathbf{k} \cdot \mathbf{p}$ Hamiltonians produce a band structure that is significantly closer to DFT results, than the standard $\mathbf{k} \cdot \mathbf{p}$ Hamiltonians. The use of extended Hamiltonians is necessary in many practical cases. If one wishes to study only the low field electrical properties or the optical properties at photon energies just above the band gap, the standard Hamiltonians are usually sufficient. However, if one is interested in optical properties in a wider energy range (which is relevant, for example, for solar cells) or transport at larger electrical fields (which is relevant in field-effect transistors) extended Hamiltonians are required to properly describe all relevant electronic states.

For the results presented so far, the $\mathbf{k} \cdot \mathbf{p}$ Hamiltonian was constructed starting from the wave functions and energies of Kohn-Sham orbitals obtained from DFT using the PBEsol

functional. It is well known that the DFT band gap is typically significantly smaller from experimental gap and for this reason the same applies to $\mathbf{k} \cdot \mathbf{p}$ band structure obtained starting from DFT wave functions and energies. The methodology that we described is by no means limited to using the DFT wave functions and energies. To demonstrate this, we have calculated the self-energy corrections to energies $E_n(\mathbf{k}_0)$ within the $G_0 W_0$ approximation. The $G_0 W_0$ calculation gives the band gap values of 1.77 and 1.60 eV without and with inclusion of spin-orbit interaction, respectively. These results are in good agreement with experimental value of 1.71 eV [39]. As expected, this is a great improvement over DFT, which underestimates the gap at 0.47 eV (without spin-orbit interaction) and 0.40 eV (with spin-orbit interaction).

The energies $E_n(\mathbf{k}_0)$ obtained from $G_0 W_0$ calculation were then used in Eqs. (10) and (8) to construct the standard and extended $\mathbf{k} \cdot \mathbf{p}$ Hamiltonian. The parameters of these Hamiltonians are given in Secs. III G and III H of Ref. [30], while the band structure obtained from diagonalization of these Hamiltonians is presented in Fig. 4.
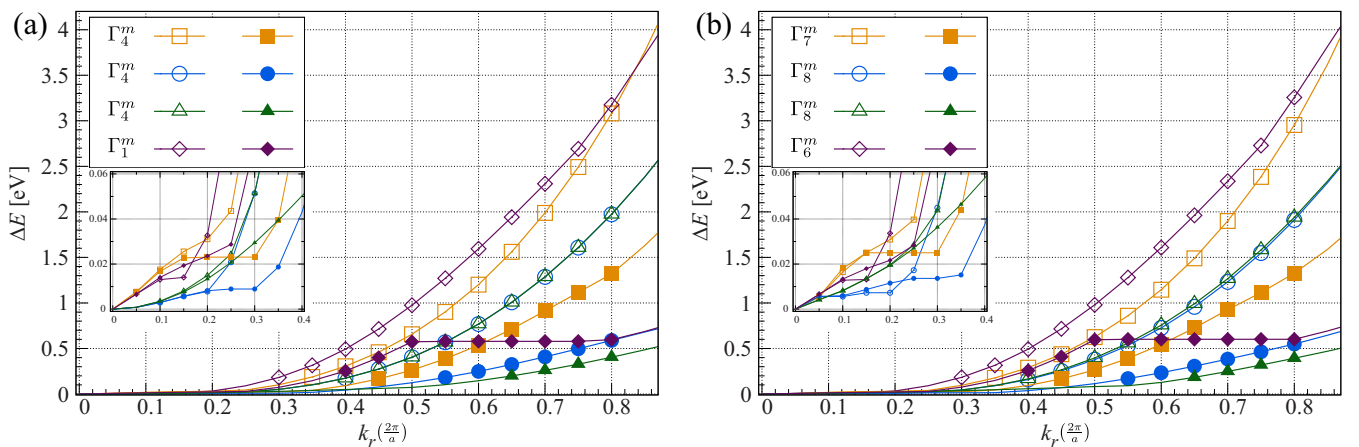


FIG. 3. Maximal absolute difference $\Delta E$ between the band energy obtained from DFT and $\mathbf{k} \cdot \mathbf{p}$ within the region of the Brillouin zone in the shape of a sphere of radius $k_r$ centered at $\Gamma$ when the effects of spin-orbit interaction are (a) omitted; (b) included. The difference is shown for main bands where the results obtained using standard $\mathbf{k} \cdot \mathbf{p}$ Hamiltonian are shown using empty symbols, while the results obtained using the extended $\mathbf{k} \cdot \mathbf{p}$ Hamiltonian are shown using filled symbols. Insets show a zoom of the same graph in the region around $k_r = 0$.
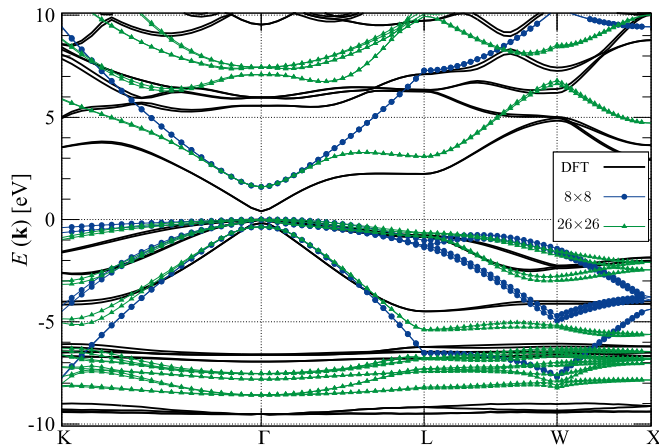
FIG. 4. Band structure of zinc-blende CdSe calculated using standard and extended $\mathbf{k} \cdot \mathbf{p}$ Hamiltonian parametrized starting from band energies obtained in $G_0W_0$ calculation. DFT results are given for comparison.

## B. CdSe quantum well

We finally demonstrate the usefulness of the procedure developed and the Hamiltonians derived by applying them to calculate the electronic states in zinc-blende CdSe quantum wells of various well widths. We perform the calculation both using the $\mathbf{k} \cdot \mathbf{p}$ method and using DFT and we compare the results that we obtain using the two approaches.

Within DFT, we perform the calculation of electronic states of a quantum well by considering the slab of CdSe material whose surfaces are perpendicular to the [001] direction. We terminate the slab with Cd layer at both surfaces and add pseudohydrogen atoms of charge 1.5 to passivate the dangling bonds at surfaces. Pseudohydrogen atoms are positioned at a distance of 1.58 Å from the corresponding Cd atom. For slabs of the width $\leqslant 6a$ ($>6a$), the vacuum region of the width equal to $3a$ (half of the slab width) was added on both sides of the quantum well, to avoid the interaction of the quantum well with its images caused by periodic boundary conditions in the calculation. The calculation was performed for quantum wells containing from 1 to 18 CdSe unit cells. We define the quantum well width as the distance between the two pseudohydrogen passivating layers. We performed the calculation without the effect of spin-orbit interaction included to lower the computational cost and therefore extend the range of well widths for comparison of DFT and $\mathbf{k} \cdot \mathbf{p}$ results.

In the case of a quantum well whose plane is perpendicular to the $z$ direction, electronic states within the $\mathbf{k} \cdot \mathbf{p}$ model can be obtained by solving the eigenvalue problem

$$\sum_n H_{mn}\left(k_x, k_y, -i\frac{d}{dz}\right)\Psi_n^{(a)}(z) = E^{(a)}\Psi_m^{(a)}(z), \qquad (16)$$

where $H_{mn}(k_x, k_y, -i\frac{d}{dz})$ is the $\mathbf{k} \cdot \mathbf{p}$ Hamiltonian of the bulk with $k_z$ component of the wave vector replaced by the differential operator $-i\frac{d}{dz}$, $\Psi_n^{(a)}(z)$ is the envelope function corresponding to the state $(a)$ of band $n$, while $E^{(a)}$ is the energy of that state. We solve the eigenvalue problem using the plane wave expansion method [40–45]. The well is embedded in the
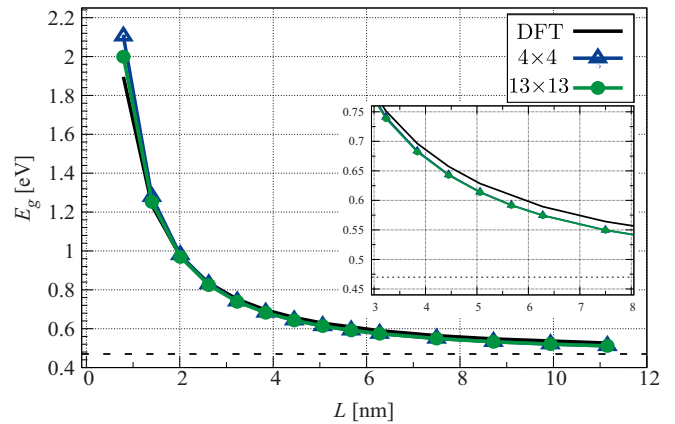


FIG. 5. Dependence of zinc-blende CdSe quantum well band gap on well width. The results obtained from DFT without the effects of spin-orbit coupling and from standard $4 \times 4$ and extended $13 \times 13$ $\mathbf{k} \cdot \mathbf{p}$ models are presented. The inset shows the zoom of the same dependence to the narrower range in the figure. The horizontal dashed line denotes the bulk DFT band gap.

region of length $L_z$ and the envelope functions are expanded into a linear combination of plane waves

$$\Psi_n^{(a)}(z) = \frac{1}{\sqrt{L_z}}\sum_{n_z=-N_z}^{N_z} c_{n,n_z}^{(a)} e^{i\frac{2\pi}{L_z}n_z z}, \qquad (17)$$

where $c_{n,n_z}^{(a)}$ are expansion coefficients that have to be determined and $N_z$ is an integer that defines the total number of plane waves. After substitution of Eq. (17) into Eq. (16) we obtain the eigenvalue problem of the Hermitian matrix that we diagonalize using standard numerical routines to obtain the coefficients $c_{n,n_z}^{(a)}$ and the energies $E^{(a)}$. For a fair comparison with DFT calculation of CdSe slab in vacuum, we perform the calculation for a quantum well inside a large energy barrier. We therefore model the region outside the quantum well as an artificial material whose all parameters are the same as CdSe parameters except the band energies at the $\Gamma$ point. In this artificial material, we increase all energies of conduction bands by $\Delta E$ with respect to corresponding energies in CdSe and decrease all energies of valence bands by the same amount $\Delta E$. In the calculation we use the values $\Delta E = 5$ eV, $L_z = 20$ nm and $N_z = 50$. We have checked that these are sufficiently large values whose further increase would not affect the results.

In Fig. 5 we present the dependence of the band gap on well width obtained within DFT and within the $\mathbf{k} \cdot \mathbf{p}$ model. For a fair comparison, the results of DFT calculation without the effects of spin-orbit interaction were compared with $\mathbf{k} \cdot \mathbf{p}$ models without spin-orbit interaction; the $4 \times 4$ and the $13 \times 13$ model. The agreement between DFT and $\mathbf{k} \cdot \mathbf{p}$ results and between the results of the two $\mathbf{k} \cdot \mathbf{p}$ models is excellent. For quantum well widths of three lattice constants and larger the band gap differences are smaller than 20 meV. The agreement is quite satisfactory even for rather thin wells of 1 and 2 unit cells, where one might not have expected that $\mathbf{k} \cdot \mathbf{p}$ performs so well. It is also important to note that the calculation of electronic structure of the quantum well using the $\mathbf{k} \cdot \mathbf{p}$ approach takes only up to a few seconds on a single-core desktop

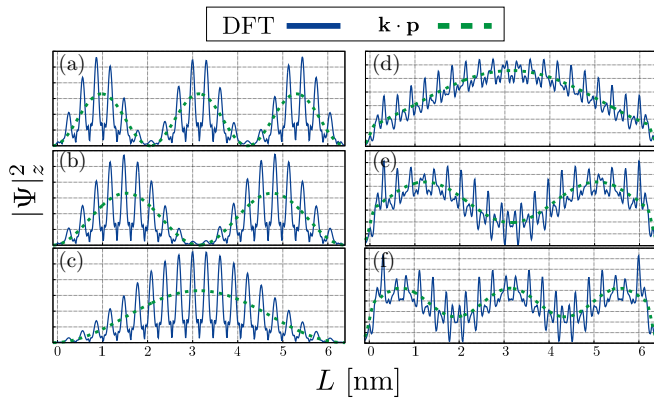FIG. 6. The wave-function moduli squared of quantum well states obtained from DFT without the effects of spin-orbit coupling and the four-band $\mathbf{k} \cdot \mathbf{p}$ model. The DFT wave functions are presented by performing the in-plane average of wave-function moduli squared. The $\mathbf{k} \cdot \mathbf{p}$ wave functions are presented by a sum $\sum_n |\Psi_n(z)|^2$. The wave functions that are presented in the figure correspond to the following states: (a) VBM-4, (b) degenerate VBM-3 and VBM-2, (c) degenerate VBM-1 and VBM, (d) CBM, (e) CBM + 1, (f) CBM + 2, where VBM (valence band maximum) denotes the highest energy state in the valence band, while CBM (conduction band minimum) denotes the lowest energy state in the conduction band.

computer, regardless of the width of the quantum well. DFT calculations, however, take minutes or hours depending on the width of the quantum well on a computing cluster with several nodes. For example, our calculation times range from approximately 3 min (using 32 cores) to 21 h (using 64 cores) for narrowest and widest quantum wells calculated by DFT, respectively. In the case of nanostructures confined in all three spatial directions, such as quantum dots, the advantages of $\mathbf{k} \cdot \mathbf{p}$ over DFT become even more pronounced. Due to a lack of periodicity in any direction, one needs to calculate supercells with quite a large number of atoms in DFT and the problem becomes computationally intractable for DFT. On the other hand, $\mathbf{k} \cdot \mathbf{p}$ is almost routinely used to study quantum dots, see for example, Refs. [40–45].

We next discuss the origin of somewhat surprisingly good agreement between DFT and $\mathbf{k} \cdot \mathbf{p}$ for thin wells. Within $\mathbf{k} \cdot \mathbf{p}$ the atomistic wave function (shown in Fig. 6 in full lines) is represented in terms of the product of slowly varying envelope functions (shown in Fig. 6 in dashed lines) and rapidly varying bulk Bloch functions, while the only additional approximation in $\mathbf{k} \cdot \mathbf{p}$ with respect to the atomistic method (DFT in our case) comes from truncation of the wave-function expansion to a limited set of bands. For this reason, we believe that excellent agreement between $\mathbf{k} \cdot \mathbf{p}$ and DFT results for wide wells is expected because basis functions used in $\mathbf{k} \cdot \mathbf{p}$ provide a good basis set in this case. In the case of very thin wells, one could argue that the representation of the wave function in terms of the product of envelope functions and bulk Bloch functions for a few bands only cannot be a good representation because the system is rather different from bulk and therefore the basis formed from bulk Bloch functions cannot be a good basis. Our results for CdSe wells confirm that such an argument is certainly valid to some extent because the agreement between
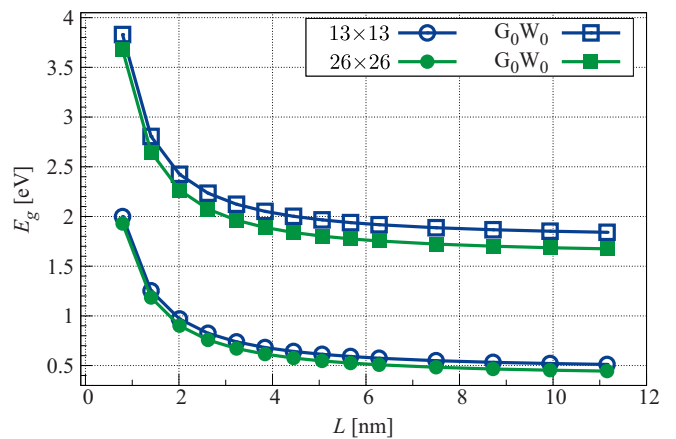


FIG. 7. Well width dependence of zinc-blende CdSe quantum well band gap calculated using the $\mathbf{k} \cdot \mathbf{p}$ method. The parameters of the $\mathbf{k} \cdot \mathbf{p}$ Hamiltonian were extracted from $G_0W_0$ calculation of bulk band structure. The results obtained with and without the effects of spin-orbit interaction are shown, respectively, in full and empty squares. The results obtained from $\mathbf{k} \cdot \mathbf{p}$ Hamiltonians parametrized from DFT are shown for comparison in full (the case with spin-orbit interaction) and empty (the case without spin-orbit interaction) circles.

DFT and $\mathbf{k} \cdot \mathbf{p}$ becomes somewhat worse for quite thin wells. Nevertheless, we find that the agreement between DFT and $\mathbf{k} \cdot \mathbf{p}$ is quite satisfactory even then and we note that it would be quite interesting to investigate in the future if this is also the case for other materials. It should be noted as well that the use of pseudohydrogen surface passivation also contributes in making the wave functions of thin wells closer to wave functions of bulk material.

We finally present the results of the calculation of CdSe quantum well electronic states, using the $\mathbf{k} \cdot \mathbf{p}$ Hamiltonians parametrized from $G_0W_0$ calculation of bulk band structure (the parameters of these Hamiltonians are given in Secs. III F and III H of Ref. [30]). To obtain an accurate quasiparticle band gap, we add to the band gap obtained from $\mathbf{k} \cdot \mathbf{p}$ Hamiltonian the correction which takes into account the dielectric mismatch between the quantum well and the vacuum, i.e., the image charge effect. The correction was added using the analytical formula presented in Ref. [46], which was also recently applied in a DFT study of CdSe nanoplatelets [47]. The results obtained are presented in Fig. 7 along with the results obtained from $\mathbf{k} \cdot \mathbf{p}$ Hamiltonians parametrized from DFT, which are given for comparison. As expected, we obtain significantly larger band gaps using $\mathbf{k} \cdot \mathbf{p}$ Hamiltonians parametrized from $G_0W_0$ calculation of bulk. We note that we focused in this work on single particle energies and the reported gaps are the quasiparticle band gaps. To obtain the optical gap, one would additionally need to consider excitonic effects, which was also recently done for CdSe nanoplatelets in Ref. [47].

## IV. CONCLUSION

In conclusion, we presented the method that allows automatic construction of $\mathbf{k} \cdot \mathbf{p}$ Hamiltonians in their symmetry-adapted form starting from output of *ab initio* band structure calculation of bulk material. We then presented

the application of the method to construct the $\mathbf{k} \cdot \mathbf{p}$ Hamiltonians for zinc-blende CdSe material. These Hamiltonians were subsequently used to calculate the electronic states in CdSe quantum wells. Interestingly, excellent agreement was obtained between the results obtained from $\mathbf{k} \cdot \mathbf{p}$ and DFT calculations of quantum wells, even for rather thin wells. While construction and parametrization of $\mathbf{k} \cdot \mathbf{p}$ Hamiltonians is usually believed to be a rather difficult and time consuming task, we expect that the method that we presented will change this situation and that it will be straightforward in the future to obtain $\mathbf{k} \cdot \mathbf{p}$ Hamiltonians for new materials and apply them to study electronic properties of nanostructures based on these materials without the need to perform any kind of fitting.

[1] J. P. Perdew, Density functional theory and the band gap problem, Int. J. Quantum Chem. **28**, 497 (1985).

[2] J. P. Perdew, M. Ernzerhof, and K. Burke, Rationale for mixing exact exchange with density functional approximations, J. Chem. Phys. **105**, 9982 (1996).

[3] C. Adamo and V. Barone, Toward reliable density functional methods without adjustable parameters: The PBE0 model, J. Chem. Phys. **110**, 6158 (1999).

[4] L. Hedin, New method for calculating the one-particle Green's function with application to the electron-gas problem, Phys. Rev. **139**, A796 (1965).

[5] M. Shishkin and G. Kresse, Self-consistent *GW* calculations for semiconductors and insulators, Phys. Rev. B **75**, 235102 (2007).

[6] W. Chen and A. Pasquarello, Band-edge levels in semiconductors and insulators: Hybrid density functional theory versus many-body perturbation theory, Phys. Rev. B **86**, 035134 (2012).

[7] Y. Hinuma, Y. Kumagai, I. Tanaka, and F. Oba, Band alignment of semiconductors and insulators using dielectric-dependent hybrid functionals: Toward high-throughput evaluation, Phys. Rev. B **95**, 075302 (2017).

[8] J. M. Luttinger and W. Kohn, Motion of electrons and holes in perturbed periodic fields, Phys. Rev. **97**, 869 (1955).

[9] E. Kane, Energy band structure in p-type germanium and silicon, J. Phys. Chem. Solids **1**, 82 (1956).

[10] C. R. Pidgeon and R. N. Brown, Interband magneto-absorption and Faraday rotation in InSb, Phys. Rev. **146**, 575 (1966).

[11] L. C. Lew Yan Voon and M. Willatzen, *The $\mathbf{k} \cdot \mathbf{p}$ Method: Electronic Properties of Semiconductors* (Springer-Verlag, Berlin, 2009).

[12] M. H. Weiler, R. L. Aggarwal, and B. Lax, Warping- and inversion-asymmetry-induced cyclotron-harmonic transitions in InSb, Phys. Rev. B **17**, 3269 (1978).

[13] T. B. Bahder, Eight-band $k \cdot p$ model of strained zinc-blende crystals, Phys. Rev. B **41**, 11992 (1990).

[14] I. Vurgaftman, J. R. Meyer, and L. R. Ram-Mohan, Band parameters for III-V compound semiconductors and their alloys, J. Appl. Phys. **89**, 5815 (2001).

[15] I. Vurgaftman and J. R. Meyer, Band parameters for nitrogen-containing semiconductors, J. Appl. Phys. **94**, 3675 (2003).

[16] M. El Kurdi, G. Fishman, S. Sauvage, and P. Boucaud, Band structure and optical gain of tensile-strained germanium based on a 30 band $k \cdot p$ formalism, J. Appl. Phys. **107**, 013710 (2010).

[17] S. Richard, F. Aniel, and G. Fishman, Energy-band structure of Ge, Si, and GaAs: A thirty-band $\mathbf{k} \cdot \mathbf{p}$ method, Phys. Rev. B **70**, 235204 (2004).

[18] S. Boyer-Richard, F. Raouafi, A. Bondi, L. Pédesseau, C. Katan, J.-M. Jancu, and J. Even, 30-band $k \cdot p$ method for quantum semiconductor heterostructures, Appl. Phys. Lett. **98**, 251913 (2011).

[19] Z. Song, W. Fan, C. S. Tan, Q. Wang, D. Nam, D. H. Zhang, and G. Sun, Band structure of Ge$_{1-x}$Sn$_x$ alloy: A full-zone 30-band $k \cdot p$ model, New J. Phys. **21**, 073037 (2019).

[20] N. A. Čukarić, M. Ž. Tadić, B. Partoens, and F. M. Peeters, 30-band $\mathbf{k} \cdot \mathbf{p}$ model of electron and hole states in silicon quantum wells, Phys. Rev. B **88**, 205306 (2013).

[21] C. E. Pryor and M.-E. Pistol, Atomistic $k \cdot p$ theory, J. Appl. Phys. **118**, 225702 (2015).

[22] C. Persson and C. Ambrosch-Draxl, A full-band FPLAPW + $k \cdot p$-method for solving the Kohn-Sham equation, Comput. Phys. Commun. **177**, 280 (2007).

[23] K. Berland and C. Persson, Enabling accurate first-principle calculations of electronic properties with a corrected $k \cdot p$ scheme, Comput. Mater. Sci. **134**, 17 (2017).

[24] T. Shishidou and T. Oguchi, $\mathbf{k} \cdot \mathbf{p}$ formula for use with linearized augmented plane waves, Phys. Rev. B **78**, 245107 (2008).

[25] C. J. Pickard and M. C. Payne, Extrapolative approaches to Brillouin-zone integration, Phys. Rev. B **59**, 4685 (1999).

[26] P. Löwdin, A note on the quantum-mechanical perturbation theory, J. Chem. Phys. **19**, 1396 (1951).

[27] M. I. Aroyo, A. Kirov, C. Capillas, J. M. Perez-Mato, and H. Wondratschek, Bilbao Crystallographic Server. II. Representations of crystallographic point groups and space groups, Acta Crystallogr. Sect. A **62**, 115 (2006).

[28] M. Mozrzymas, M. Studziński, and M. Horodecki, Explicit constructions of unitary transformations between equivalent irreducible representations, J. Phys. A **47**, 505203 (2014).

[29] J. M. Luttinger, Quantum theory of cyclotron resonance in semiconductors: General theory, Phys. Rev. **102**, 1030 (1956).

[30] See Supplemental Material at http://link.aps.org/supplemental/10.1103/PhysRevB.102.085121 for characters of irreducible representations of the $T_d$ group, analytical expressions for the elements of all blocks of the $\mathbf{k} \cdot \mathbf{p}$ Hamiltonians and numerical values of the parameters of the Hamiltonians.

[31] J. P. Perdew, A. Ruzsinszky, G. I. Csonka, O. A. Vydrov, G. E. Scuseria, L. A. Constantin, X. Zhou, and K. Burke, Restoring the Density-Gradient Expansion for Exchange in Solids and Surfaces, Phys. Rev. Lett. **100**, 136406 (2008).

[32] P. Giannozzi, S. Baroni, N. Bonini, M. Calandra, R. Car, C. Cavazzoni, D. Ceresoli, G. L. Chiarotti, M. Cococcioni, I. Dabo, A. Dal Corso, S. de Gironcoli, S. Fabris, G. Fratesi, R. Gebauer, U. Gerstmann, C. Gougoussis, A. Kokalj, M. Lazzeri, L. Martin-Samos, N. Marzari, F. Mauri, R. Mazzarello, S. Paolini, A. Pasquarello, L. Paulatto, C. Sbraccia, S. Scandolo, G. Sclauzero, A. P. Seitsonen, A. Smogunov, P. Umari, and R. M. Wentzcovitch, QUANTUM ESPRESSO: A modular and open-source software project for quantum simulations of materials, J. Phys.: Condens. Matter **21**, 395502 (2009).

[33] P. Giannozzi, O. Andreussi, T. Brumme, O. Bunau, M. B. Nardelli, M. Calandra, R. Car, C. Cavazzoni, D. Ceresoli, M. Cococcioni, N. Colonna, I. Carnimeo, A. D. Corso, S. de Gironcoli, P. Delugas, R. A. D. Jr, A. Ferretti, A. Floris, G. Fratesi, G. Fugallo, R. Gebauer, U. Gerstmann, F. Giustino, T. Gorni, J. Jia, M. Kawamura, H.-Y. Ko, A. Kokalj, E. Kucukbenli, M. Lazzeri, M. Marsili, N. Marzari, F. Mauri, N. L. Nguyen, H.-V. Nguyen, A. O. de-la Roza, L. Paulatto, S. Poncé, D. Rocca, R. Sabatini, B. Santra, M. Schlipf, A. P. Seitsonen, A. Smogunov, I. Timrov, T. Thonhauser, P. Umari, N. Vast, X. Wu, and S. Baroni, Advanced capabilities for materials modeling with Quantum ESPRESSO, J. Phys.: Condens. Matter **29**, 465901 (2017).

[34] D. R. Hamann, Optimized norm-conserving Vanderbilt pseudopotentials, Phys. Rev. B **88**, 085117 (2013).

[35] M. van Setten, M. Giantomassi, E. Bousquet, M. Verstraete, D. Hamann, X. Gonze, and G.-M. Rignanese, The pseudodojo: Training and grading a 85 element optimized norm-conserving pseudopotential table, Comp. Phys. Comm. **226**, 39 (2018).

[36] D. Sangalli, A. Ferretti, H. Miranda, C. Attaccalite, I. Marri, E. Cannuccia, P. Melo, M. Marsili, F. Paleari, A. Marrazzo, G. Prandini, P. Bonfà, M. O. Atambo, F. Affinito, M. Palummo, A. Molina-Sánchez, C. Hogan, M. Grüning, D. Varsano, and A.

Marini, Many-body perturbation theory calculations using the Yambo code, J. Phys.: Condens. Matter **31**, 325902 (2019).

[37] A. Marini, C. Hogan, M. Grüning, and D. Varsano, Yambo: An *ab initio* tool for excited state calculations, Comp. Phys. Comm. **180**, 1392 (2009).

[38] A. P. Cracknell, B. L. Davies, S. C. Miller, and W. F. Love, *Kronecker Product Tables, 1, General Introduction and Tables of Irreducible Representations of Space groups* (IFI/Plenum, New York, 1979).

[39] S. Ninomiya and S. Adachi, Optical properties of cubic and hexagonal CdSe, J. Appl. Phys. **78**, 4681 (1995).

[40] M. A. Cusack, P. R. Briddon, and M. Jaros, Electronic structure of InAs/GaAs self-assembled quantum dots, Phys. Rev. B **54**, R2300 (1996).

[41] S.-S. Li, J.-B. Xia, Z. L. Yuan, Z. Y. Xu, W. Ge, X. R. Wang, Y. Wang, J. Wang, and L. L. Chang, Effective-mass theory for InAs/GaAs strained coupled quantum dots, Phys. Rev. B **54**, 11575 (1996).

[42] A. D. Andreev and E. P. O'Reilly, Theory of the electronic structure of GaN/AlN hexagonal quantum dots, Phys. Rev. B **62**, 15851 (2000).

[43] S. Tomić, A. G. Sunderland, and I. J. Bush, Parallel multi-band **k** · **p** code for electronic structure of zinc blend semiconductor quantum dots, J. Mater. Chem. **16**, 1963 (2006).

[44] N. Vukmirović, D. Indjin, V. D. Jovanović, Z. Ikonić, and P. Harrison, Symmetry of **k** · **p** Hamiltonian in pyramidal InAs/GaAs quantum dots: Application to the calculation of electronic structure, Phys. Rev. B **72**, 075356 (2005).

[45] N. Vukmirović and S. Tomić, Plane wave methodology for single quantum dot electronic structure calculations, J. Appl. Phys. **103**, 103718 (2008).

[46] Y. Cho and T. C. Berkelbach, Environmentally sensitive theory of electronic and optical transitions in atomically thin semiconductors, Phys. Rev. B **97**, 041409(R) (2018).

[47] Q. Zhou, Y. Cho, S. Yang, E. A. Weiss, T. C. Berkelbach, and P. Darancet, Large band edge tunability in colloidal nanoplatelets, Nano Lett. **19**, 7124 (2019).

# Supplementary material for: Ab-initio construction of symmetry-adapted $\mathbf{k} \cdot \mathbf{p}$ Hamiltonians for electronic structure of semiconductors

Milan Jocić[*] and Nenad Vukmirović[†]

*Institute of Physics Belgrade, University of Belgrade, Pregrevica 118, 11080 Belgrade, Serbia*

[*] milan.jocic@ipb.ac.rs

[†] nenad.vukmirovic@ipb.ac.rs

# I. CHARACTER TABLES OF THE $T_d$ POINT SINGLE AND DOUBLE GROUP

| $T_d$ | E | $3C_2$ | $6S_4$ | $6\sigma_d$ | $8C_3$ |
|---|---|---|---|---|---|
| $\Gamma_1$ $(A_1)$ $x^2+y^2+z^2$ | 1 | 1 | 1 | 1 | 1 |
| $\Gamma_2$ $(A_2)$ | 1 | 1 | -1 | -1 | 1 |
| $\Gamma_3$ $(E)$ $(x^2-y^2,$ $3z^2-r^2)$ | 2 | 2 | 0 | 0 | -1 |
| $\Gamma_4$ $(T_2)$ $(z,x,y)$ | 3 | -1 | -1 | 1 | 0 |
| $\Gamma_5$ $(T_1)$ $(xy,yz,zx)$ | 3 | -1 | 1 | -1 | 0 |

TABLE I. Character table for the $T_d$ point group [1, 2].

| $T_d$ | E | $3C_2$ $3\overline{C}_2$ | $6S_4$ | $6\sigma_d$ $6\overline{\sigma}_d$ | $8C_3$ | $\overline{E}$ | $6\overline{S}_4$ | $8\overline{C}_3$ |
|---|---|---|---|---|---|---|---|---|
| $\Gamma_1$ $(A_1)$ $x^2+y^2+z^2$ | 1 | 1 | 1 | 1 | 1 | 1 | 1 | 1 |
| $\Gamma_2$ $(A_2)$ | 1 | 1 | -1 | -1 | 1 | 1 | -1 | 1 |
| $\Gamma_3$ $(E)$ $(x^2-y^2,$ $3z^2-r^2)$ | 2 | 2 | 0 | 0 | -1 | 2 | 0 | -1 |
| $\Gamma_4$ $(T_2)$ $(z,x,y)$ | 3 | -1 | -1 | 1 | 0 | 3 | -1 | 0 |
| $\Gamma_5$ $(T_1)$ $(xy,yz,zx)$ | 3 | -1 | 1 | -1 | 0 | 3 | 1 | 0 |
| $\Gamma_6$ $(\overline{E}_1)$ | 2 | 0 | $\sqrt{2}$ | 0 | 1 | -2 | $-\sqrt{2}$ | -1 |
| $\Gamma_7$ $(\overline{E}_2)$ | 2 | 0 | $-\sqrt{2}$ | 0 | 1 | -2 | $\sqrt{2}$ | -1 |
| $\Gamma_8$ $(\overline{F})$ | 4 | 0 | 0 | 0 | -1 | -4 | 0 | 1 |

TABLE II. Character table for the double $T_d$ point group [1].

## II. ANALYTICAL EXPRESSIONS FOR THE ELEMENTS OF ALL BLOCKS OF THE $\mathbf{k} \cdot \mathbf{p}$ HAMILTONIAN

In this section, we list the Hamiltonian matrix elements arising from the term $\frac{\hbar(\mathbf{k}-\mathbf{k}_0)}{m_0} \cdot \langle \Psi_{n\mathbf{k}_0} | \mathbf{p} | \Psi_{m\mathbf{k}_0} \rangle$ in Eq. (8) and the $H_{nm}^{(2)}$ term in Eq. (10) of the main part of the paper. To obtain the full $\mathbf{k} \cdot \mathbf{p}$ Hamiltonian these terms should be complemented with the diagonal term $\left[ E_n(\mathbf{k}_0) + \frac{\hbar^2(\mathbf{k}-\mathbf{k}_0)^2}{2m_0} \right] \delta_{nm}$.

### A. Single group $T_d$

We now list analytical expressions for all possible blocks $\mathcal{B}(\Gamma_m, \Gamma_n)$ of the $\mathbf{k} \cdot \mathbf{p}$ Hamiltonian in the case of single $T_d$ group:

$$\mathcal{B}(\Gamma_1, \Gamma_1) = C_1 k^2, \tag{1}$$

$$\mathcal{B}(\Gamma_1, \Gamma_2) = 0, \tag{2}$$

$$\mathcal{B}(\Gamma_1, \Gamma_3) = C_2 \left[ (k_z^2 + \omega^2 k_x^2 + \omega k_y^2) \ (k_z^2 + \omega k_x^2 + \omega^2 k_y^2) \right], \quad \omega = e^{i2\pi/3}, \tag{3}$$

$$\mathcal{B}(\Gamma_1, \Gamma_4) = C_3 \left[ k_z \ k_x \ k_y \right] + C_4 \left[ k_x k_y \ k_y k_z \ k_z k_x \right], \tag{4}$$

$$\mathcal{B}(\Gamma_1, \Gamma_5) = 0, \tag{5}$$

$$\mathcal{B}(\Gamma_2, \Gamma_2) = C_5 k^2, \tag{6}$$

$$\mathcal{B}(\Gamma_2, \Gamma_3) = C_6 \left[ -(k_z^2 + \omega^2 k_x^2 + \omega k_y^2) \ (k_z^2 + \omega k_x^2 + \omega^2 k_y^2) \right], \tag{7}$$

$$\mathcal{B}(\Gamma_2, \Gamma_4) = 0, \tag{8}$$

$$\mathcal{B}(\Gamma_2, \Gamma_5) = C_7 \left[ k_z \ k_x \ k_y \right] + C_8 \left[ k_x k_y \ k_y k_z \ k_z k_x \right], \tag{9}$$

$$\mathcal{B}(\Gamma_3, \Gamma_3) = C_9 \begin{bmatrix} k^2 & 0 \\ 0 & k^2 \end{bmatrix}$$
$$+ C_{10} \begin{bmatrix} 0 & (k_z^2 + \omega^2 k_x^2 + \omega k_y^2) \\ (k_z^2 + \omega k_x^2 + \omega^2 k_y^2) & 0 \end{bmatrix}, \tag{10}$$

$$\mathcal{B}(\Gamma_3, \Gamma_4) = C_{11} \begin{bmatrix} k_z & \omega k_x & \omega^2 k_y \\ k_z & \omega^2 k_x & \omega k_y \end{bmatrix}$$
$$+ C_{12} \begin{bmatrix} k_x k_y & \omega k_y k_z & \omega^2 k_z k_x \\ k_x k_y & \omega^2 k_y k_z & \omega k_z k_x \end{bmatrix}, \tag{11}$$

$$\mathcal{B}(\Gamma_3, \Gamma_5) = C_{13} \begin{bmatrix} k_z & \omega k_x & \omega^2 k_y \\ -k_z & -\omega^2 k_x & -\omega k_y \end{bmatrix}$$
$$+ C_{14} \begin{bmatrix} k_x k_y & \omega k_y k_z & \omega^2 k_z k_x \\ -k_x k_y & -\omega^2 k_y k_z & -\omega k_z k_x \end{bmatrix} \tag{12}$$

$$\mathcal{B}(\Gamma_4, \Gamma_4) = C_{15} \begin{bmatrix} 0 & k_y & k_x \\ k_y & 0 & k_z \\ k_x & k_z & 0 \end{bmatrix}$$
$$+ C_{16} \begin{bmatrix} 0 & k_z k_x & k_y k_z \\ k_z k_x & 0 & k_x k_y \\ k_y k_z & k_x k_y & 0 \end{bmatrix}$$
$$+ C_{17} \begin{bmatrix} 2k_z^2 - k_x^2 - k_y^2 & 0 & 0 \\ 0 & 2k_x^2 - k_y^2 - k_z^2 & 0 \\ 0 & 0 & 2k_y^2 - k_z^2 - k_x^2 \end{bmatrix}$$
$$+ C_{18} \begin{bmatrix} k^2 & 0 & 0 \\ 0 & k^2 & 0 \\ 0 & 0 & k^2 \end{bmatrix}, \tag{13}$$

$$\mathcal{B}(\Gamma_4, \Gamma_5) = C_{19} \begin{bmatrix} 0 & k_y & -k_x \\ -k_y & 0 & k_z \\ k_x & -k_z & 0 \end{bmatrix}$$
$$+ C_{20} \begin{bmatrix} 0 & k_z k_x & -k_y k_z \\ -k_z k_x & 0 & k_x k_y \\ k_y k_z & -k_x k_y & 0 \end{bmatrix}$$
$$+ C_{21} \begin{bmatrix} k_x^2 - k_y^2 & 0 & 0 \\ 0 & k_y^2 - k_z^2 & 0 \\ 0 & 0 & k_z^2 - k_x^2 \end{bmatrix}, \tag{14}$$

$$\mathcal{B}(\Gamma_5, \Gamma_5) = C_{22} \begin{bmatrix} 0 & k_y & k_x \\ k_y & 0 & k_z \\ k_x & k_z & 0 \end{bmatrix}$$
$$+ C_{23} \begin{bmatrix} 0 & k_z k_x & k_y k_z \\ k_z k_x & 0 & k_x k_y \\ k_y k_z & k_x k_y & 0 \end{bmatrix}$$
$$+ C_{24} \begin{bmatrix} 2k_z^2 - k_x^2 - k_y^2 & 0 & 0 \\ 0 & 2k_x^2 - k_y^2 - k_z^2 & 0 \\ 0 & 0 & 2k_y^2 - k_z^2 - k_x^2 \end{bmatrix}$$
$$+ C_{25} \begin{bmatrix} k^2 & 0 & 0 \\ 0 & k^2 & 0 \\ 0 & 0 & k^2 \end{bmatrix}, \tag{15}$$

To form the $\mathbf{k} \cdot \mathbf{p}$ Hamiltonian based on a chosen set of bands, one should simply combine all relevant blocks. For example, to obtain the 4×4 Hamiltonian based on the $\Gamma_1^m$ and $\Gamma_4^m$ bands, one should take the blocks $\mathcal{B}(\Gamma_1, \Gamma_1)$,

$\mathcal{B}(\Gamma_1, \Gamma_4)$, $\mathcal{B}(\Gamma_4, \Gamma_1)$ and $\mathcal{B}(\Gamma_4, \Gamma_4)$. The Hamiltonian that we obtain in this case (taking into account that $C_{15} = 0$ as shown in Section III A) corresponds exactly to the second-order four-band Kane Hamiltonian [3].

It is common in the literature to choose the states that transform as $x$, $y$ and $z$ as the basis of the three-dimensional manifold of $\Gamma_4$ states. On the other hand, we pointed out at the end of Section II-B in the main part of the paper that this basis $|\psi_i\rangle$ [Eq. (13) of the paper] depends on the convention for matrices of irreps, $\Gamma_4$ in this case. We find that the convention for matrices of irrep $\Gamma_4$ that we used leads exactly to the basis states that transform as $x$, $y$ and $z$. For this reason, we obtain the form of the Hamiltonian that is identical to the second-order four-band Kane Hamiltonian which is formulated in $x$, $y$, $z$ basis.

## B. Double group $T_d$

When spin-orbit interaction is included, the states transform according to the representations of the double point group $T_d$, which means that only the $\Gamma_6, \Gamma_7$ and $\Gamma_8$ states are relevant. Since the matrices that we obtained have some parts that appear more than once, we introduce the following shortened notation:

$$\Upsilon = \omega^2 k_x^2 + \omega k_y^2 + k_z^2, \tag{16}$$

$$\Sigma(z, x, y) = \begin{bmatrix} z & x - iy \\ x + iy & -z \end{bmatrix}, \tag{17}$$

$$\Delta(z, x, y) = \begin{bmatrix} ze^{i45°} & xe^{-i75°} + ye^{i75°} \\ xe^{-i75°} + ye^{-i105°} & ze^{-i135°} \end{bmatrix}, \tag{18}$$

$$\Lambda(z, x, y) = \begin{bmatrix} xe^{i30°} + ye^{i60°} & z \\ ze^{i90°} & xe^{i120°} + ye^{-i30°} \end{bmatrix}, \tag{19}$$

$$\Xi(z, x, y) = \begin{bmatrix} ze^{-i135°} & xe^{i105°} + ye^{-i105°} \\ xe^{i105°} + ye^{i75°} & ze^{i45°} \end{bmatrix}. \tag{20}$$

$$\Omega_1(z, x, y) = \begin{bmatrix} xe^{i60°} + ye^{-i150°} & -iz \\ z & xe^{i150°} + ye^{i120°} \end{bmatrix}$$

$$\Omega_2(z, x, y) = \begin{bmatrix} xe^{i30°} + ye^{-i120°} & iz \\ -z & xe^{-i60°} + ye^{-i30°} \end{bmatrix} \tag{21}$$

Using the notation from equations (16) through (21) we write down the relevant blocks of the Hamiltonian in case of double point group $T_d$:

$$\mathcal{B}(\Gamma_6, \Gamma_6) = C_1^d k^2, \tag{22}$$

$$\mathcal{B}(\Gamma_7, \Gamma_7) = C_2^d k^2, \tag{23}$$

$$\mathcal{B}(\Gamma_6, \Gamma_7) = C_3^d \Sigma(k_z, k_x, k_y) + C_4^d \Sigma(k_x k_y, k_y k_z, k_z k_x) \tag{24}$$

$$\mathcal{B}(\Gamma_6, \Gamma_8) = C_5^d \begin{bmatrix} -\frac{1+i}{2}\Upsilon & 0 & 0 & \frac{1}{\sqrt{2}}\Upsilon^* \\ 0 & -\frac{1+i}{2}\Upsilon & -\frac{i}{\sqrt{2}}\Upsilon^* & 0 \end{bmatrix}$$
$$+ C_6^d \left[ \Delta(k_z, k_x, k_y) \quad \Lambda(k_z, k_x, k_y) \right]$$
$$+ C_7^d \left[ \Delta(k_x k_y, k_y k_z, k_z k_x) \quad \Lambda(k_x k_y, k_y k_z, k_z k_x) \right] \tag{25}$$

$$\mathcal{B}(\Gamma_7, \Gamma_8) = +C_8^d \begin{bmatrix} \frac{1+i}{2}\Upsilon & 0 & 0 & \frac{1}{\sqrt{2}}\Upsilon^* \\ 0 & \frac{1+i}{2}\Upsilon & -\frac{i}{\sqrt{2}}\Upsilon^* & 0 \end{bmatrix}$$
$$+ C_9^d \left[ \Xi(k_z, k_x, k_y) \quad \Lambda(k_z, k_x, k_y) \right]$$
$$+ C_{10}^d \left[ \Xi(k_x k_y, k_y k_z, k_z k_x) \quad \Lambda(k_x k_y, k_y k_z, k_z k_x) \right], \tag{26}$$

$$\mathcal{B}(\Gamma_8, \Gamma_8) = C_{11}^d k^2$$
$$+ C_{12}^d \begin{bmatrix} 0 & 0 & 0 & -\Upsilon \\ 0 & 0 & i\Upsilon & 0 \\ 0 & \Upsilon^* & 0 & 0 \\ -i\Upsilon^* & 0 & 0 & 0 \end{bmatrix}$$
$$+ C_{13}^d \begin{bmatrix} \Sigma(k_z, k_x, k_y) & 0 \\ 0 & \Sigma(k_z, k_y, k_x) \end{bmatrix}$$
$$+ C_{14}^d \begin{bmatrix} 0 & \Omega_1(k_z, k_x, k_y) \\ \Omega_2(k_z, k_x, k_y) & 0 \end{bmatrix}$$
$$+ C_{15}^d \begin{bmatrix} \Sigma(k_x k_y, k_y k_z, k_z k_x) & 0 \\ 0 & \Sigma(k_x k_y, k_z k_x, k_y k_z) \end{bmatrix}$$
$$+ C_{16}^d \begin{bmatrix} 0 & \Omega_1(k_x k_y, k_y k_z, k_z k_x) \\ \Omega_2(k_x k_y, k_y k_z, k_z k_x) & 0 \end{bmatrix}, \tag{27}$$

It is common in the literature to choose the states that transform as $1/2$ angular momentum states in the two-dimensional manifolds of $\Gamma_6$ and $\Gamma_7$ states and the states that transform as $3/2$ angular momentum states in the four-dimensional manifold of $\Gamma_8$ states. On the other hand, we pointed out at the end of Section II-B in the main part of the paper that the basis $|\psi_i\rangle$ [Eq. (13) of the paper] in these manifolds depends on the convention for matrices of irreps, $\Gamma_6$-$\Gamma_8$ in this case. We find that the convention for matrices of irreps $\Gamma_6$ and $\Gamma_7$ that we used leads exactly to the basis states that transform as $1/2$ angular momentum states. However, the convention for matrices of irrep $\Gamma_8$ does not yield the basis states that transform as $3/2$ angular momentum states. For this reason, we do not get the same form of Hamiltonian that is obtained in the literature when the basis of $3/2$ angular momentum states is used.

In particular, the 8-band Hamiltonian that we obtain by taking the highest valence bands that transform as $\Gamma_7$ and $\Gamma_8$ and the lowest conduction band that transforms as $\Gamma_6$ coincides with Weiler 8-band Hamiltonian [3, 4] only after an appropriate unitary transformation is made. This unitary transformation consists of a transformation to $3/2$ angular momentum basis in the $\Gamma_8$ manifold and additionally it has some trivial phase factor multiplications (the terms $e^{j\phi_1}$ and $e^{j\phi_2}$). The transformation is given as

$$H_8' = U^\dagger H_8 U. \tag{28}$$

In this equation $H_8$ is the eight-band Hamiltonian that we obtain from our procedure and $H_8'$ is the 8-band Hamiltonian

reported in Ref. [4] (also reproduced in Ref. [3]). The matrix $U$ reads

$$
U = \begin{bmatrix}
0 & 0 & 0 & 0 & 0 & 0 & 0 & e^{j\phi_1} \\
0 & 0 & 0 & e^{j\phi_1} & 0 & 0 & 0 & 0 \\
0 & 0 & 0 & 0 & 0 & \frac{\sqrt{2}}{2} & \frac{j\sqrt{2}}{2} & 0 \\
0 & -\frac{j\sqrt{2}}{2} & -\frac{\sqrt{2}}{2} & 0 & 0 & 0 & 0 & 0 \\
0 & -\frac{1}{2}-\frac{j}{2} & \frac{1}{2}-\frac{j}{2} & 0 & 0 & 0 & 0 & 0 \\
0 & 0 & 0 & 0 & 0 & \frac{1}{2}+\frac{j}{2} & \frac{1}{2}-\frac{j}{2} & 0 \\
e^{j\phi_2} & 0 & 0 & 0 & 0 & 0 & 0 & 0 \\
0 & 0 & 0 & 0 & e^{j\phi_2} & 0 & 0 & 0
\end{bmatrix}. \tag{29}
$$

The phase factors $e^{j\phi_1}$ and $e^{j\phi_2}$ adjust the phases so that all parameters of the Weiler Hamiltonian become real. For the parameters given in Section III C these phase factors read $e^{j\phi_1} = 0.93659+0.35042\cdot j$ and $e^{j\phi_2} = -0.98853-0.15103\cdot j$. After performing the transformation given in Eq. (28) we obtain the Weiler Hamiltonian with parameters (for the parameters given in Section III C): $\gamma_1 = 3.82622$, $\gamma_2 = -0.32116$, $\gamma_3 = 0.39693$, $\gamma_1' = 3.84008$, $\gamma_2' = -0.28179$, $\gamma_3' = 0.43182$, $P = 0.40682$, $P' = 0.38616$, $G = 0.26536$, $G' = 0.00000$, $F = 0.12078$, $C = -0.00931$, $C' = -0.00042$, $N_2 = 0.02090$. These parameters were given in Hartree atomic units.

We have also checked that our procedure yields directly the Weiler Hamiltonian (up to phase factors $e^{j\phi_1}$ and $e^{j\phi_2}$ that need to be fixed) if we use from the beginning the matrices of irrep $\Gamma_8$ that transform as $3/2$ angular momentum states.

## C.  Comparison of DFT-obtained and symmetry-adapted $4 \times 4$ Hamiltonian

Two analytical forms of the $4 \times 4$ Hamiltonian, made from degenerate states corresponding to $\Gamma_4$ and $\Gamma_1$ irreps that lie below and above the gap respectively, in the case of CdSe, are presented here. Both Hamiltonians give the same physics, overall, and they are connected by an unitary transformation $U$, that is used to transform initial DFT basis $|\phi_i\rangle$ to the symmetry-adapted basis $|\psi_j\rangle$. To give more clarity and justify the whole procedure of transforming the initial DFT basis, we will compare inital DFT-form $H_{\mathrm{DFT}}^{\mathrm{init}}$, obtained from groups of degenerate states $|\phi_i\rangle$ and symmetry-adapted form $H_{\mathrm{adap}}^{\mathrm{sym}}$, that is made out of transformed groups of degenerate states $|\psi_j\rangle$.

Initial DFT-form $H_{\mathrm{DFT}}^{\mathrm{init}}$ of the $4 \times 4$ Hamiltonian is given as:

$$
H_{\mathrm{DFT}}^{\mathrm{init}} = \frac{\hbar^2 k^2}{2m_0} + \begin{bmatrix} E_{\Gamma_4} & 0 & 0 & 0 \\ 0 & E_{\Gamma_4} & 0 & 0 \\ 0 & 0 & E_{\Gamma_4} & 0 \\ 0 & 0 & 0 & E_{\Gamma_1} \end{bmatrix} + \frac{\hbar}{m_0} \begin{bmatrix} 0 & 0 & 0 & P_{03}^{(1)} \\ 0 & 0 & 0 & P_{13}^{(1)} \\ 0 & 0 & 0 & P_{23}^{(1)} \\ P_{03}^{(1)*} & P_{13}^{(1)*} & P_{23}^{(1)*} & 0 \end{bmatrix} + \frac{\hbar^2}{m_0^2} \begin{bmatrix} P_{00}^{(2)} & P_{01}^{(2)} & P_{02}^{(2)} & P_{03}^{(2)} \\ P_{01}^{(2)*} & P_{11}^{(2)} & P_{12}^{(2)} & P_{13}^{(2)} \\ P_{02}^{(2)*} & P_{12}^{(2)*} & P_{22}^{(2)} & P_{23}^{(2)} \\ P_{03}^{(2)*} & P_{13}^{(2)*} & P_{23}^{(2)*} & P_{33}^{(2)} \end{bmatrix},
$$

where:

$$
\begin{aligned}
P_{i3}^{(1)} &= C_{i3}^{x(1)} k_x + C_{i3}^{y(1)} k_y + C_{i3}^{z(1)} k_z, \quad i = 0, 1, 2; \\
P_{i3}^{(2)} &= C_{i3}^{xy(2)} k_x k_y + C_{i3}^{yz(2)} k_y k_z + C_{i3}^{zx(2)} k_z k_x, \quad i = 0, 1, 2; \\
P_{ij}^{(2)} &= C_{ij}^{xx(2)} k_x^2 + C_{ij}^{yy(2)} k_y^2 + C_{ij}^{zz(2)} k_z^2 + C_{ij}^{xy(2)} k_x k_y + C_{ij}^{yz(2)} k_y k_z + C_{ij}^{zx(2)} k_z k_x, \quad i,j = 0, 1, 2; \\
P_{33}^{(2)} &= C_{33}^{zz(2)} k^2.
\end{aligned}
$$

If we count the number of parameters $C_{i3}^{m(1)}$ for 1st order and $C_{ij}^{mn(2)}$ for 2nd order terms $(m, n = x, y, z)$ in the last four expressions, we can tell that $H_{\mathrm{DFT}}^{\mathrm{init}}$ has a total number of $3 \times 3 + 3 \times 3 + 6 \times 6 + 1 = 55$ parameters. Of course, this number can be reduced but the procedure could be rather cumbersome especially if a great number of materials with different symmetries is considered.

Symmetry-adapted form $H_{\mathrm{adap}}^{\mathrm{sym}}$ of the $4 \times 4$ Hamiltonian is given as:

$$
\begin{aligned}
H_{\mathrm{adap}}^{\mathrm{sym}} = {}& \frac{\hbar^2 k^2}{2m_0} + \begin{bmatrix} E_{\Gamma_4} & 0 & 0 & 0 \\ 0 & E_{\Gamma_4} & 0 & 0 \\ 0 & 0 & E_{\Gamma_4} & 0 \\ 0 & 0 & 0 & E_{\Gamma_1} \end{bmatrix} + \frac{\hbar}{m_0} \begin{bmatrix} 0 & C_{15} k_y & C_{15} k_x & C_3 k_z \\ C_{15} k_y & 0 & C_{15} k_z & C_3 k_x \\ C_{15} k_x & C_{15} k_z & 0 & C_3 k_y \\ C_3^* k_z & C_3^* k_x & C_3^* k_y & 0 \end{bmatrix} \\
& + \frac{\hbar^2}{m_0^2} \begin{bmatrix} C_{17}(2k_z^2 - k_x^2 - k_y^2) + C_{18} k^2 & C_{16} k_z k_x & C_{16} k_y k_z & C_4^* k_x k_y \\ C_{16} k_z k_x & C_{17}(2k_x^2 - k_y^2 - k_z^2) + C_{18} k^2 & C_{16} k_x k_y & C_4^* k_y k_z \\ C_{16} k_y k_z & C_{16} k_x k_y & C_{17}(2k_y^2 - k_z^2 - k_x^2) + C_{18} k^2 & C_4^* k_z k_x \\ C_4 k_x k_y & C_4 k_y k_z & C_4 k_z k_x & C_1 k^2 \end{bmatrix},
\end{aligned}
$$

where $C_{15} = 0$ if the block is formed from two same $\Gamma_4$ irreps as it is in the $4 \times 4$ case. This gives for $H_{\mathrm{adap}}^{\mathrm{sym}}$, a total number of $1 + 5 = 6$ parameters, for 1st and 2nd order $\mathbf{k} \cdot \mathbf{p}$ terms. This way, if we were to consider a large number of crystals, we could group them according to their symmetry group, and compare the individual parameters.

Unlike symmetry-adapted form $H_{\mathrm{adap}}^{\mathrm{sym}}$, initial DFT-form $H_{\mathrm{DFT}}^{\mathrm{init}}$ clearly demonstrates much more parameters than symmetry of the crystal CdSe would suggest, even for the simplest $4 \times 4$ case.

# III.   NUMERICAL VALUES OF THE PARAMETERS

In this Section, we present the numerical values of the parameters of the Hamiltonians obtained. All quantities are given in Hartree atomic units, while relevant energies are additionally also given in electron volts. Table  III gives a summary of different parametrizations of the Hamiltonian and the sections where the parametrizations are given.

| Section | Hamiltonian |
|---|---|
| Section III A | Standard 4×4 Hamiltonian parametrized from DFT without SOC |
| Section III B | Extended 13×13 Hamiltonian parametrized from DFT without SOC |
| Section III C | Standard 8×8 Hamiltonian parametrized from DFT with SOC |
| Section III D | Extended 26×26 Hamiltonian parametrized from DFT with SOC |
| Section III E | Standard 4×4 Hamiltonian parametrized from DFT without SOC with quasiparticle energies taken from $G_0W_0$ calculation |
| Section III F | Extended 13×13 Hamiltonian parametrized from DFT without SOC with quasiparticle energies taken from $G_0W_0$ calculation |
| Section III G | Standard 8×8 Hamiltonian parametrized from DFT with SOC with quasiparticle energies taken from $G_0W_0$ calculation |
| Section III H | Extended 26×26 Hamiltonian parametrized from DFT with SOC with quasiparticle energies taken from $G_0W_0$ calculation |

TABLE III. A summary of different parametrizations of the Hamiltonian and the sections where the parametrizations are given.

## A. Standard 4×4 Hamiltonian

|  | E[eV] | E[Hartree] |
|---|---|---|
| $\Gamma_4^m$ | 0.0 | 0.0 |
| $\Gamma_1^m$ | 0.46821 | 0.01721 |

|  | $\mathcal{B}(\Gamma_1^m, \Gamma_1^m)$ |
|---|---|
| $C_1$ | 0.03880 |

|  | $\mathcal{B}(\Gamma_1^m, \Gamma_4^m)$ |
|---|---|
| $C_3$ | $0.29213 + 0.28073j$ |
| $C_4$ | $0.22183 - 0.23083j$ |

|  | $\mathcal{B}(\Gamma_4^m, \Gamma_4^m)$ |
|---|---|
| $C_{15}$ | 0 |
| $C_{16}$ | -0.68794 |
| $C_{17}$ | 0.16303 |
| $C_{18}$ | -1.04656 |

## B. Extended 13×13 Hamiltonian

|            | E[eV]    | E[Hartree] |
|------------|----------|------------|
| $\Gamma_4^v$ | -7.88140 | -0.28964   |
| $\Gamma_3^v$ | -7.50786 | -0.27591   |
| $\Gamma_4^m$ | 0.0      | 0.0        |
| $\Gamma_1^m$ | 0.46821  | 0.01721    |
| $\Gamma_4^c$ | 5.87086  | 0.21575    |
| $\Gamma_1^c$ | 9.58302  | 0.35217    |

|       | $\mathcal{B}(\Gamma_1^m,\Gamma_1^m)$ | $\mathcal{B}(\Gamma_1^c,\Gamma_1^c)$ | $\mathcal{B}(\Gamma_1^c,\Gamma_1^m)$ |
|-------|---------|---------|----------------------|
| $C_1$ | 0.01616 | 0.01635 | $-0.00653 - 0.03685j$ |

|       | $\mathcal{B}(\Gamma_1^c,\Gamma_3^v)$ | $\mathcal{B}(\Gamma_1^m,\Gamma_3^v)$ |
|-------|----------------------|----------------------|
| $C_2$ | $-0.13097 - 0.07961j$ | $0.10099 - 0.11476j$ |

|       | $\mathcal{B}(\Gamma_1^m,\Gamma_4^v)$ | $\mathcal{B}(\Gamma_1^m,\Gamma_4^m)$ | $\mathcal{B}(\Gamma_1^m,\Gamma_4^c)$ |
|-------|----------------------|----------------------|----------------------|
| $C_3$ | $-0.16939 - 0.05120j$ | $0.29213 + 0.28073j$ | $-0.12171 + 0.03090j$ |
| $C_4$ | $-0.09935 + 0.32871j$ | $-0.08738 + 0.09093j$ | $-0.00165 - 0.00649j$ |

|       | $\mathcal{B}(\Gamma_1^c,\Gamma_4^v)$ | $\mathcal{B}(\Gamma_1^c,\Gamma_4^m)$ | $\mathcal{B}(\Gamma_1^c,\Gamma_4^c)$ |
|-------|----------------------|----------------------|----------------------|
| $C_3$ | $0.00690 - 0.05817j$ | $0.00911 - 0.01361j$ | $0.23220 + 0.51426j$ |
| $C_4$ | $0.41908 + 0.04970j$ | $0.12813 + 0.08580j$ | $0.00524 - 0.00237j$ |

|          | $\mathcal{B}(\Gamma_3^v,\Gamma_3^v)$ |
|----------|-----------|
| $C_9$    | $-0.33898$ |
| $C_{10}$ | $0.12786$  |

|          | $\mathcal{B}(\Gamma_3^v,\Gamma_4^v)$ | $\mathcal{B}(\Gamma_3^v,\Gamma_4^m)$ | $\mathcal{B}(\Gamma_3^v,\Gamma_4^c)$ |
|----------|----------------------|----------------------|----------------------|
| $C_{11}$ | $0.00272 + 0.00595j$ | $0.00154 - 0.03508j$ | $-0.19430 - 0.13307j$ |
| $C_{12}$ | $0.12304 - 0.05616j$ | $0.03769 + 0.00165j$ | $-0.06773 + 0.09889j$ |

|          | $\mathcal{B}(\Gamma_4^v,\Gamma_4^v)$ | $\mathcal{B}(\Gamma_4^m,\Gamma_4^m)$ | $\mathcal{B}(\Gamma_4^c,\Gamma_4^c)$ |
|----------|----------|----------|----------|
| $C_{15}$ | 0        | 0        | 0        |
| $C_{16}$ | 0.29432  | 0.39888  | $-0.47968$ |
| $C_{17}$ | $-0.00204$ | $-0.20023$ | 0.07955  |
| $C_{18}$ | $-0.29136$ | $-0.32823$ | $-0.55226$ |

|          | $\mathcal{B}(\Gamma_4^m,\Gamma_4^v)$ | $\mathcal{B}(\Gamma_4^c,\Gamma_4^v)$ | $\mathcal{B}(\Gamma_4^c,\Gamma_4^m)$ |
|----------|----------------------|----------------------|----------------------|
| $C_{15}$ | $0.05946 + 0.11647j$ | $0.03891 - 0.06460j$ | $0.42118 - 0.26210j$ |
| $C_{16}$ | $-0.16023 + 0.08180j$ | $0.15739 + 0.09480j$ | $-0.08474 - 0.13617j$ |
| $C_{17}$ | $-0.02788 + 0.01423j$ | $-0.04879 - 0.02939j$ | $0.08051 + 0.12937j$ |
| $C_{18}$ | $-0.16355 + 0.08349j$ | $0.03718 + 0.02240j$ | $0.06582 + 0.10577j$ |

## C.  Standard 8×8 Hamiltonian

|  | E[eV] | E[Hartree] |
|---|---|---|
| $\Gamma_7^m$ | -0.16924 | -0.00622 |
| $\Gamma_8^m$ | 0.0 | 0.0 |
| $\Gamma_6^m$ | 0.40085 | 0.01473 |

|  | $\mathcal{B}(\Gamma_6^m, \Gamma_6^m)$ |
|---|---|
| $C_1^d$ | 0.06588 |

|  | $\mathcal{B}(\Gamma_7^m, \Gamma_7^m)$ |
|---|---|
| $C_2^d$ | $-1.04722$ |

|  | $\mathcal{B}(\Gamma_6^m, \Gamma_7^m)$ |
|---|---|
| $C_3^d$ | $-0.21822 + 0.04568j$ |
| $C_4^d$ | $0.03234 + 0.15448j$ |

|  | $\mathcal{B}(\Gamma_6^m, \Gamma_8^m)$ |
|---|---|
| $C_5^d$ | $0.01350 + 0.01837j$ |
| $C_6^d$ | $0.18927 - 0.13908j$ |
| $C_7^d$ | $-0.09896 - 0.13467j$ |

|  | $\mathcal{B}(\Gamma_7^m, \Gamma_8^m)$ |
|---|---|
| $C_8^d$ | $-0.19781 + 0.09009j$ |
| $C_9^d$ | $-0.00009 - 0.00019j$ |
| $C_{10}^d$ | $0.37124 - 0.16908j$ |

|  | $\mathcal{B}(\Gamma_8^m, \Gamma_8^m)$ |
|---|---|
| $C_{11}^d$ | $-1.04344$ |
| $C_{12}^d$ | $-0.12387 + 0.12387j$ |
| $C_{13}^d$ | $0$ |
| $C_{14}^d$ | $-0.00658 + 0.00658j$ |
| $C_{15}^d$ | $-0.37497$ |
| $C_{16}^d$ | $0$ |

## D. Extended 26×26 Hamiltonian

|  | E[eV] | E[Hartree] |
|---|---|---|
| $\Gamma_8^{v_1}$ | -9.50287 | -0.34922 |
| $\Gamma_7^v$ | -6.94697 | -0.25530 |
| $\Gamma_8^{v_2}$ | -6.60685 | -0.24280 |
| $\Gamma_7^m$ | -0.16924 | -0.00622 |
| $\Gamma_8^m$ | 0.0 | 0.0 |
| $\Gamma_6^m$ | 0.40085 | 0.01473 |
| $\Gamma_7^c$ | 5.56618 | 0.20455 |
| $\Gamma_8^c$ | 5.97379 | 0.21953 |
| $\Gamma_6^c$ | 9.53629 | 0.35045 |

|  | $\mathcal{B}(\Gamma_6^m,\Gamma_6^m)$ | $\mathcal{B}(\Gamma_6^c,\Gamma_6^m)$ | $\mathcal{B}(\Gamma_6^c,\Gamma_6^c)$ |
|---|---|---|---|
| $C_1^d$ | 0.01863 | $0.02546 + 0.03002j$ | 0.01738 |

|  | $\mathcal{B}(\Gamma_7^v,\Gamma_7^v)$ | $\mathcal{B}(\Gamma_7^m,\Gamma_7^v)$ | $\mathcal{B}(\Gamma_7^c,\Gamma_7^v)$ |
|---|---|---|---|
| $C_2^d$ | $-0.26310$ | $0.15491 + 0.11684j$ | $0.02861 - 0.02945j$ |

|  | $\mathcal{B}(\Gamma_7^m,\Gamma_7^m)$ | $\mathcal{B}(\Gamma_7^c,\Gamma_7^m)$ | $\mathcal{B}(\Gamma_7^c,\Gamma_7^c)$ |
|---|---|---|---|
| $C_2^d$ | $-0.36390$ | $-0.01605 + 0.12791j$ | $-0.51997$ |

|  | $\mathcal{B}(\Gamma_6^m,\Gamma_7^v)$ | $\mathcal{B}(\Gamma_6^m,\Gamma_7^m)$ | $\mathcal{B}(\Gamma_6^m,\Gamma_7^c)$ |
|---|---|---|---|
| $C_3^d$ | $-0.10904 - 0.05132j$ | $-0.21822 + 0.04568j$ | $-0.02093 - 0.06086j$ |
| $C_4^d$ | $-0.08139 + 0.17295j$ | $-0.01709 - 0.08162j$ | $-0.00481 + 0.00165j$ |

|  | $\mathcal{B}(\Gamma_6^c,\Gamma_7^v)$ | $\mathcal{B}(\Gamma_6^c,\Gamma_7^m)$ | $\mathcal{B}(\Gamma_6^c,\Gamma_7^c)$ |
|---|---|---|---|
| $C_3^d$ | $0.00855 + 0.03169j$ | $-0.01216 - 0.00946j$ | $0.16439 - 0.27667j$ |
| $C_4^d$ | $-0.22411 + 0.06048j$ | $0.06612 - 0.08502j$ | $-0.01687 - 0.01002j$ |

|  | $\mathcal{B}(\Gamma_6^m,\Gamma_8^{v_1})$ | $\mathcal{B}(\Gamma_6^m,\Gamma_8^{v_2})$ |
|---|---|---|
| $C_5^d$ | $-0.08794 - 0.08322j$ | $-0.15106 + 0.08260j$ |
| $C_6^d$ | $0.04906 - 0.05184j$ | $0.03470 + 0.06346j$ |
| $C_7^d$ | $-0.11283 - 0.10676j$ | $0.10096 - 0.05520j$ |

|  | $\mathcal{B}(\Gamma_6^m,\Gamma_8^m)$ | $\mathcal{B}(\Gamma_6^m,\Gamma_8^c)$ |
|---|---|---|
| $C_5^d$ | $-0.00953 - 0.01296j$ | $-0.00537 + 0.00572j$ |
| $C_6^d$ | $0.18927 - 0.13908j$ | $0.05385 + 0.05061j$ |
| $C_7^d$ | $0.04030 + 0.05485j$ | $-0.00588 + 0.00626j$ |

| | $\mathcal{B}(\Gamma_6^c, \Gamma_8^{v1})$ | $\mathcal{B}(\Gamma_6^c, \Gamma_8^{v2})$ |
|---|---|---|
| $C_5^d$ | $0.00696 - 0.12794j$ | $-0.15674 - 0.06024j$ |
| $C_6^d$ | $-0.02513 - 0.00137j$ | $0.00701 - 0.01823j$ |
| $C_7^d$ | $0.01060 - 0.19485j$ | $0.13521 + 0.05197j$ |

| | $\mathcal{B}(\Gamma_6^c, \Gamma_8^m)$ | $\mathcal{B}(\Gamma_6^c, \Gamma_8^c)$ |
|---|---|---|
| $C_5^d$ | $0.00378 - 0.01590j$ | $-0.02377 - 0.00121j$ |
| $C_6^d$ | $0.00866 + 0.00206j$ | $-0.01685 + 0.33051j$ |
| $C_7^d$ | $-0.01955 + 0.08214j$ | $-0.01545 - 0.00079j$ |

| | $\mathcal{B}(\Gamma_7^v, \Gamma_8^{v1})$ | $\mathcal{B}(\Gamma_7^v, \Gamma_8^{v2})$ |
|---|---|---|
| $C_8^d$ | $0.00039 - 0.00117j$ | $-0.00096 - 0.00070j$ |
| $C_9^d$ | $0.00272 + 0.00090j$ | $-0.00280 + 0.00384j$ |
| $C_{10}^d$ | $-0.03069 + 0.09326j$ | $-0.13829 - 0.10095j$ |

| | $\mathcal{B}(\Gamma_7^v, \Gamma_8^m)$ | $\mathcal{B}(\Gamma_7^v, \Gamma_8^c)$ |
|---|---|---|
| $C_8^d$ | $-0.01475 + 0.02717j$ | $0.08938 + 0.02908j$ |
| $C_9^d$ | $-0.06796 - 0.03688j$ | $0.00602 - 0.01850j$ |
| $C_{10}^d$ | $-0.05483 + 0.10103j$ | $-0.11487 - 0.03737j$ |

| | $\mathcal{B}(\Gamma_7^m, \Gamma_8^{v1})$ | $\mathcal{B}(\Gamma_7^m, \Gamma_8^{v2})$ |
|---|---|---|
| $C_8^d$ | $-0.03485 + 0.02419j$ | $-0.00500 - 0.01650j$ |
| $C_9^d$ | $0.02810 + 0.04050j$ | $-0.06265 + 0.01897j$ |
| $C_{10}^d$ | $-0.07114 + 0.04937j$ | $-0.01250 - 0.04129j$ |

| | $\mathcal{B}(\Gamma_7^m, \Gamma_8^m)$ | $\mathcal{B}(\Gamma_7^m, \Gamma_8^c)$ |
|---|---|---|
| $C_8^d$ | $0.25682 - 0.11697j$ | $0.11600 + 0.16596j$ |
| $C_9^d$ | $-0.00009 - 0.00019j$ | $-0.23577 + 0.16480j$ |
| $C_{10}^d$ | $-0.20194 + 0.09197j$ | $-0.04193 - 0.05999j$ |

| | $\mathcal{B}(\Gamma_7^c, \Gamma_8^{v1})$ | $\mathcal{B}(\Gamma_7^c, \Gamma_8^{v2})$ |
|---|---|---|
| $C_8^d$ | $-0.02450 - 0.04686j$ | $0.05328 - 0.00910j$ |
| $C_9^d$ | $0.10802 - 0.05649j$ | $-0.01634 - 0.09568j$ |
| $C_{10}^d$ | $0.05044 + 0.09647j$ | $-0.00961 + 0.00164j$ |

| | $\mathcal{B}(\Gamma_7^c, \Gamma_8^m)$ | $\mathcal{B}(\Gamma_7^c, \Gamma_8^c)$ |
|---|---|---|
| $C_8^d$ | $-0.06033 - 0.19331j$ | $-0.09941 + 0.05241j$ |
| $C_9^d$ | $-0.26218 + 0.08183j$ | $-0.00437 - 0.00829j$ |
| $C_{10}^d$ | $0.02882 + 0.09235j$ | $0.24092 - 0.12702j$ |

| | $\mathcal{B}(\Gamma_8^{v1}, \Gamma_8^{v1})$ | $\mathcal{B}(\Gamma_8^{v2}, \Gamma_8^{v1})$ |
|---|---|---|
| $C_{11}^d$ | $-0.28902$ | $-0.00696 - 0.02152j$ |
| $C_{12}^d$ | $0.02918 - 0.02918j$ | $0.05393 + 0.02759j$ |
| $C_{13}^d$ | $0$ | $-0.00655 + 0.00212j$ |
| $C_{14}^d$ | $-0.00148 + 0.00148j$ | $-0.00064 - 0.00033j$ |
| $C_{15}^d$ | $0.18072$ | $-0.01765 - 0.05462j$ |
| $C_{16}^d$ | $0$ | $-0.03641 + 0.07119j$ |

| | $\mathcal{B}(\Gamma_8^m, \Gamma_8^{v_1})$ | $\mathcal{B}(\Gamma_8^c, \Gamma_8^{v_1})$ |
|---|---|---|
| $C_{11}^d$ | $0.13348 - 0.02419j$ | $0.00012 - 0.03541j$ |
| $C_{12}^d$ | $-0.01469 + 0.02119j$ | $-0.02594 - 0.02611j$ |
| $C_{13}^d$ | $-0.01220 - 0.06732j$ | $0.03234 + 0.00011j$ |
| $C_{14}^d$ | $-0.00593 + 0.00856j$ | $-0.05535 - 0.05573j$ |
| $C_{15}^d$ | $0.06877 - 0.01246j$ | $0.00014 - 0.03990j$ |
| $C_{16}^d$ | $0.01221 + 0.00846j$ | $0.02512 - 0.02495j$ |

| | $\mathcal{B}(\Gamma_8^{v_2}, \Gamma_8^{v_2})$ | $\mathcal{B}(\Gamma_8^m, \Gamma_8^{v_2})$ |
|---|---|---|
| $C_{11}^d$ | $-0.30823$ | $-0.01543 + 0.11501j$ |
| $C_{12}^d$ | $0.05971 - 0.05971j$ | $-0.01187 - 0.01555j$ |
| $C_{13}^d$ | $0$ | $0.02416 + 0.00324j$ |
| $C_{14}^d$ | $0.00399 - 0.00399j$ | $0.01190 + 0.01558j$ |
| $C_{15}^d$ | $-0.01283$ | $-0.01215 + 0.09055j$ |
| $C_{16}^d$ | $0$ | $0.00727 - 0.00555j$ |

| | $\mathcal{B}(\Gamma_8^c, \Gamma_8^{v_2})$ | $\mathcal{B}(\Gamma_8^m, \Gamma_8^m)$ |
|---|---|---|
| $C_{11}^d$ | $0.02899 + 0.00948j$ | $-0.32179$ |
| $C_{12}^d$ | $0.03694 - 0.01874j$ | $0.14004 - 0.14004j$ |
| $C_{13}^d$ | $0.03764 - 0.11510j$ | $0$ |
| $C_{14}^d$ | $-0.09818 + 0.04980j$ | $-0.00658 + 0.00658j$ |
| $C_{15}^d$ | $0.12964 + 0.04239j$ | $0.22602$ |
| $C_{16}^d$ | $-0.02793 - 0.05507j$ | $0$ |

| | $\mathcal{B}(\Gamma_8^c, \Gamma_8^m)$ | $\mathcal{B}(\Gamma_8^c, \Gamma_8^c)$ |
|---|---|---|
| $C_{11}^d$ | $-0.02317 + 0.12545j$ | $-0.57103$ |
| $C_{12}^d$ | $-0.08829 - 0.12830j$ | $-0.06365 + 0.06365j$ |
| $C_{13}^d$ | $0.28896 + 0.05338j$ | $0$ |
| $C_{14}^d$ | $-0.00592 - 0.00860j$ | $-0.00004 + 0.00004j$ |
| $C_{15}^d$ | $0.01451 - 0.07853j$ | $-0.30114$ |
| $C_{16}^d$ | $0.01504 - 0.01035j$ | $0$ |

## E. Standard 4×4 + GW

|          | E[eV]    | E[Hartree] |
|----------|----------|------------|
| $\Gamma_4^m$ | 0.0      | 0.0        |
| $\Gamma_1^m$ | 1.76931  | 0.06502    |

|       | $\mathcal{B}(\Gamma_1^m, \Gamma_1^m)$ |
|-------|---------------------------------------|
| $C_1$ | 0.02705                               |

|       | $\mathcal{B}(\Gamma_1^m, \Gamma_4^m)$ |
|-------|---------------------------------------|
| $C_3$ | $0.29213 + 0.28073j$                  |
| $C_4$ | $0.16975 - 0.17664j$                  |

|          | $\mathcal{B}(\Gamma_4^m, \Gamma_4^m)$ |
|----------|---------------------------------------|
| $C_{15}$ | 0                                     |
| $C_{16}$ | -0.47738                              |
| $C_{17}$ | 0.11355                               |
| $C_{18}$ | -0.84096                              |

**F.   Extended 13×13 + GW**

|            | E[eV]     | E[Hartree] |
|------------|-----------|------------|
| $\Gamma_4^v$ | -8.14820  | -0.29944   |
| $\Gamma_3^v$ | -7.83478  | -0.28792   |
| $\Gamma_4^m$ | 0.0       | 0.0        |
| $\Gamma_1^m$ | 1.76931   | 0.06502    |
| $\Gamma_4^c$ | 7.52506   | 0.27654    |
| $\Gamma_1^c$ | 11.16596  | 0.41034    |

|       | $\mathcal{B}(\Gamma_1^m,\Gamma_1^m)$ | $\mathcal{B}(\Gamma_1^c,\Gamma_1^c)$ | $\mathcal{B}(\Gamma_1^c,\Gamma_1^m)$ |
|-------|---------|---------|-----------------------|
| $C_1$ | 0.01567 | 0.01478 | $-0.00646 - 0.03643j$ |

|       | $\mathcal{B}(\Gamma_1^c,\Gamma_3^v)$ | $\mathcal{B}(\Gamma_1^m,\Gamma_3^v)$ |
|-------|-----------------------|-----------------------|
| $C_2$ | $-0.13113 - 0.07971j$ | $0.10078 - 0.11452j$  |

|       | $\mathcal{B}(\Gamma_1^m,\Gamma_4^v)$ | $\mathcal{B}(\Gamma_1^m,\Gamma_4^m)$ | $\mathcal{B}(\Gamma_1^m,\Gamma_4^c)$ |
|-------|-----------------------|-----------------------|-----------------------|
| $C_3$ | $-0.16939 - 0.05120j$ | $0.29213 + 0.28073j$  | $-0.12171 + 0.03090j$ |
| $C_4$ | $-0.09967 + 0.32976j$ | $-0.08734 + 0.09089j$ | $-0.00172 - 0.00677j$ |

|       | $\mathcal{B}(\Gamma_1^c,\Gamma_4^v)$ | $\mathcal{B}(\Gamma_1^c,\Gamma_4^m)$ | $\mathcal{B}(\Gamma_1^c,\Gamma_4^c)$ |
|-------|-----------------------|-----------------------|-----------------------|
| $C_3$ | $0.00690 - 0.05817j$  | $0.00911 - 0.01361$   | $0.23220 + 0.51426j$  |
| $C_4$ | $0.41786 + 0.04955j$  | $0.12719 + 0.08516j$  | $0.00359 - 0.00162j$  |

|          | $\mathcal{B}(\Gamma_3^v,\Gamma_3^v)$ |
|----------|------------|
| $C_9$    | $-0.30827$ |
| $C_{10}$ | $0.14407$  |

|          | $\mathcal{B}(\Gamma_3^v,\Gamma_4^v)$ | $\mathcal{B}(\Gamma_3^v,\Gamma_4^m)$ | $\mathcal{B}(\Gamma_3^v,\Gamma_4^c)$ |
|----------|-----------------------|-----------------------|-----------------------|
| $C_{11}$ | $0.00272 + 0.00595j$  | $0.00154 - 0.03508j$  | $-0.19430 - 0.13307j$ |
| $C_{12}$ | $0.13632 - 0.06214j$  | $0.04124 + 0.00183j$  | $-0.06481 + 0.09462j$ |

|          | $\mathcal{B}(\Gamma_4^v,\Gamma_4^v)$ | $\mathcal{B}(\Gamma_4^m,\Gamma_4^m)$ | $\mathcal{B}(\Gamma_4^c,\Gamma_4^c)$ |
|----------|------------|------------|------------|
| $C_{15}$ | 0          | 0          | 0          |
| $C_{16}$ | 0.32363    | 0.36031    | $-0.51563$ |
| $C_{17}$ | $-0.00691$ | $-0.16664$ | 0.09072    |
| $C_{18}$ | $-0.26036$ | $-0.28849$ | $-0.57456$ |

|          | $\mathcal{B}(\Gamma_4^m,\Gamma_4^v)$ | $\mathcal{B}(\Gamma_4^c,\Gamma_4^v)$ | $\mathcal{B}(\Gamma_4^c,\Gamma_4^m)$ |
|----------|-----------------------|-----------------------|-----------------------|
| $C_{15}$ | $0.05946 + 0.11647j$  | $0.03891 - 0.06460j$  | $0.42118 - 0.26210j$  |
| $C_{16}$ | $-0.15214 + 0.07767j$ | $0.14989 + 0.09029j$  | $-0.07498 - 0.12046j$ |
| $C_{17}$ | $-0.03336 + 0.01703j$ | $-0.04548 - 0.02740j$ | $0.07282 + 0.11701j$  |
| $C_{18}$ | $-0.15886 + 0.08110j$ | $0.03496 + 0.02106j$  | $0.05809 + 0.09335j$  |

## G.   Standard 8×8 + GW

|         | E[eV]    | E[Hartree] |
|---------|----------|------------|
| $\Gamma_7^m$ | -0.35663 | -0.01311   |
| $\Gamma_8^m$ | 0.0      | 0.0        |
| $\Gamma_6^m$ | 1.60110  | 0.05884    |

|         | $\mathcal{B}(\Gamma_6^m, \Gamma_6^m)$ |
|---------|----------------|
| $C_1^d$ | 0.04692        |

|         | $\mathcal{B}(\Gamma_7^m, \Gamma_7^m)$ |
|---------|----------------|
| $C_2^d$ | $-0.84410$     |

|         | $\mathcal{B}(\Gamma_6^m, \Gamma_7^m)$ |
|---------|--------------------------|
| $C_3^d$ | $-0.21822 + 0.04568j$    |
| $C_4^d$ | $0.02561 + 0.12234j$     |

|         | $\mathcal{B}(\Gamma_6^m, \Gamma_8^m)$ |
|---------|--------------------------|
| $C_5^d$ | $0.01200 + 0.01638j$     |
| $C_6^d$ | $0.18927 - 0.13908j$     |
| $C_7^d$ | $-0.07907 - 0.10747j$    |

|            | $\mathcal{B}(\Gamma_7^m, \Gamma_8^m)$ |
|------------|--------------------------|
| $C_8^d$    | $-0.14870 + 0.06776j$    |
| $C_9^d$    | $-0.00009 - 0.00019j$    |
| $C_{10}^d$ | $0.26240 - 0.11980j$     |

|            | $\mathcal{B}(\Gamma_8^m, \Gamma_8^m)$ |
|------------|--------------------------|
| $C_{11}^d$ | $-0.84342$               |
| $C_{12}^d$ | $-0.09171 + 0.09171j$    |
| $C_{13}^d$ | $0$                      |
| $C_{14}^d$ | $-0.00658 + 0.00658j$    |
| $C_{15}^d$ | $-0.25600$               |
| $C_{16}^d$ | $-0.00010 - 0.00003j$    |

## H.   Extended 26×26 + GW

|            | E[eV]    | E[Hartree] |
|------------|----------|------------|
| $\Gamma_8^{v_1}$ | -8.57873 | -0.31526   |
| $\Gamma_7^{v}$   | -7.80871 | -0.28696   |
| $\Gamma_8^{v_2}$ | -7.52888 | -0.27668   |
| $\Gamma_7^{m}$   | -0.35663 | -0.01311   |
| $\Gamma_8^{m}$   | 0.0      | 0.0        |
| $\Gamma_6^{m}$   | 1.60110  | 0.05884    |
| $\Gamma_7^{c}$   | 7.08839  | 0.26049    |
| $\Gamma_8^{c}$   | 7.45201  | 0.27386    |
| $\Gamma_6^{c}$   | 10.94474 | 0.40221    |

|         | $\mathcal{B}(\Gamma_6^m, \Gamma_6^m)$ | $\mathcal{B}(\Gamma_6^c, \Gamma_6^m)$ | $\mathcal{B}(\Gamma_6^c, \Gamma_6^c)$ |
|---------|---------|-------------------|---------|
| $C_1^d$ | 0.01787 | $0.02517 + 0.02968j$ | 0.01622 |

|         | $\mathcal{B}(\Gamma_7^v, \Gamma_7^v)$ | $\mathcal{B}(\Gamma_7^m, \Gamma_7^v)$ | $\mathcal{B}(\Gamma_7^c, \Gamma_7^v)$ |
|---------|----------|-------------------|-------------------|
| $C_2^d$ | $-0.23320$ | $0.15446 + 0.11650j$ | $0.02601 - 0.02676j$ |

|         | $\mathcal{B}(\Gamma_7^m, \Gamma_7^m)$ | $\mathcal{B}(\Gamma_7^c, \Gamma_7^m)$ | $\mathcal{B}(\Gamma_7^c, \Gamma_7^c)$ |
|---------|-----------|----------------------|-----------|
| $C_2^d$ | $-0.31525$ | $-0.01412 + 0.11250j$ | $-0.52764$ |

|         | $\mathcal{B}(\Gamma_6^m, \Gamma_7^v)$ | $\mathcal{B}(\Gamma_6^m, \Gamma_7^m)$ | $\mathcal{B}(\Gamma_6^m, \Gamma_7^c)$ |
|---------|----------------------|----------------------|----------------------|
| $C_3^d$ | $-0.10904 - 0.05132j$ | $-0.21822 + 0.04568j$ | $-0.02093 - 0.06086j$ |
| $C_4^d$ | $-0.07496 + 0.15929j$ | $-0.01593 - 0.07609j$ | $-0.00452 + 0.00155j$ |

|         | $\mathcal{B}(\Gamma_6^c, \Gamma_7^v)$ | $\mathcal{B}(\Gamma_6^c, \Gamma_7^m)$ | $\mathcal{B}(\Gamma_6^c, \Gamma_7^c)$ |
|---------|----------------------|----------------------|----------------------|
| $C_3^d$ | $0.00855 + 0.03169j$ | $-0.01216 - 0.00946j$ | $0.16439 - 0.27667j$ |
| $C_4^d$ | $-0.20847 + 0.05626j$ | $0.06220 - 0.07998j$ | $-0.01632 - 0.00970j$ |

|         | $\mathcal{B}(\Gamma_6^m, \Gamma_8^{v_1})$ | $\mathcal{B}(\Gamma_6^m, \Gamma_8^{v_2})$ |
|---------|----------------------|----------------------|
| $C_5^d$ | $-0.09464 - 0.08979j$ | $-0.14089 + 0.07718j$ |
| $C_6^d$ | $0.04906 - 0.05184j$ | $0.03470 + 0.06346j$ |
| $C_7^d$ | $-0.12041 - 0.11423j$ | $0.09121 - 0.04970j$ |

|         | $\mathcal{B}(\Gamma_6^m, \Gamma_8^m)$ | $\mathcal{B}(\Gamma_6^m, \Gamma_8^c)$ |
|---------|----------------------|----------------------|
| $C_5^d$ | $-0.00692 - 0.00935j$ | $-0.00540 + 0.00576j$ |
| $C_6^d$ | $0.18927 - 0.13908j$ | $0.05385 + 0.05061j$ |
| $C_7^d$ | $0.03989 + 0.05442j$ | $-0.00600 + 0.00639j$ |

|  | $\mathcal{B}(\Gamma_6^c, \Gamma_8^{v_1})$ | $\mathcal{B}(\Gamma_6^c, \Gamma_8^{v_2})$ |
|---|---|---|
| $C_5^d$ | $0.00764 - 0.13736j$ | $-0.14748 - 0.05656j$ |
| $C_6^d$ | $-0.02513 - 0.00137j$ | $0.00701 - 0.01823j$ |
| $C_7^d$ | $0.01135 - 0.20448j$ | $0.12410 + 0.04787j$ |

|  | $\mathcal{B}(\Gamma_6^c, \Gamma_8^m)$ | $\mathcal{B}(\Gamma_6^c, \Gamma_8^c)$ |
|---|---|---|
| $C_5^d$ | $0.00272 - 0.01162j$ | $-0.02515 - 0.00128j$ |
| $C_6^d$ | $0.00866 + 0.00206j$ | $-0.01685 + 0.33051j$ |
| $C_7^d$ | $-0.01939 + 0.08107j$ | $-0.01749 - 0.00090j$ |

|  | $\mathcal{B}(\Gamma_7^v, \Gamma_8^{v1})$ | $\mathcal{B}(\Gamma_7^v, \Gamma_8^{v2})$ |
|---|---|---|
| $C_8^d$ | $-0.00414 + 0.01232j$ | $-0.01149 - 0.00684j$ |
| $C_9^d$ | $0.00272 + 0.00090j$ | $-0.00280 + 0.00384j$ |
| $C_{10}^d$ | $-0.03263 + 0.09720j$ | $-0.13961 - 0.10233j$ |

|  | $\mathcal{B}(\Gamma_7^v, \Gamma_8^m)$ | $\mathcal{B}(\Gamma_7^v, \Gamma_8^c)$ |
|---|---|---|
| $C_8^d$ | $-0.01982 + 0.03607j$ | $0.08224 + 0.02674j$ |
| $C_9^d$ | $-0.06796 - 0.03688j$ | $0.00602 - 0.01850j$ |
| $C_{10}^d$ | $-0.05602 + 0.10399j$ | $-0.10628 - 0.03469j$ |

|  | $\mathcal{B}(\Gamma_7^m, \Gamma_8^{v1})$ | $\mathcal{B}(\Gamma_7^m, \Gamma_8^{v2})$ |
|---|---|---|
| $C_8^d$ | $-0.03271 + 0.02272j$ | $-0.00680 - 0.02378j$ |
| $C_9^d$ | $0.02810 + 0.04050j$ | $-0.06265 + 0.01897j$ |
| $C_{10}^d$ | $-0.06765 + 0.04739j$ | $-0.01399 - 0.04525j$ |

|  | $\mathcal{B}(\Gamma_7^m, \Gamma_8^m)$ | $\mathcal{B}(\Gamma_7^m, \Gamma_8^c)$ |
|---|---|---|
| $C_8^d$ | $0.20749 - 0.09443j$ | $0.10528 + 0.15070j$ |
| $C_9^d$ | $-0.00009 - 0.00019j$ | $-0.23577 + 0.16480j$ |
| $C_{10}^d$ | $-0.18687 + 0.08485j$ | $-0.03553 - 0.05067j$ |

|  | $\mathcal{B}(\Gamma_7^c, \Gamma_8^{v1})$ | $\mathcal{B}(\Gamma_7^c, \Gamma_8^{v2})$ |
|---|---|---|
| $C_8^d$ | $-0.02363 - 0.04506j$ | $0.04854 - 0.00825j$ |
| $C_9^d$ | $0.10802 - 0.05649j$ | $-0.01634 - 0.09568j$ |
| $C_{10}^d$ | $0.05062 + 0.09761j$ | $-0.00680 + 0.00146j$ |

|  | $\mathcal{B}(\Gamma_7^c, \Gamma_8^m)$ | $\mathcal{B}(\Gamma_7^c, \Gamma_8^c)$ |
|---|---|---|
| $C_8^d$ | $-0.05385 - 0.17267j$ | $-0.12004 + 0.06312j$ |
| $C_9^d$ | $-0.26218 + 0.08183j$ | $-0.00437 - 0.00829j$ |
| $C_{10}^d$ | $0.02444 + 0.07796j$ | $0.25733 - 0.13537j$ |

|  | $\mathcal{B}(\Gamma_8^{v_1}, \Gamma_8^{v_1})$ | $\mathcal{B}(\Gamma_8^{v_2}, \Gamma_8^{v_1})$ |
|---|---|---|
| $C_{11}^d$ | $-0.24713$ | $-0.00492 - 0.01847j$ |
| $C_{12}^d$ | $0.06463 - 0.06424j$ | $0.05715 + 0.02905j$ |
| $C_{13}^d$ | $0$ | $-0.00655 + 0.00212j$ |
| $C_{14}^d$ | $-0.00148 + 0.00148j$ | $-0.00064 - 0.00033j$ |
| $C_{15}^d$ | $0.25098$ | $-0.01534 - 0.04886j$ |
| $C_{16}^d$ | $0.00006 + 0.00049j$ | $-0.02898 + 0.05775j$ |

| | $\mathcal{B}(\Gamma_8^m, \Gamma_8^{v_1})$ | $\mathcal{B}(\Gamma_8^c, \Gamma_8^{v_1})$ |
|---|---|---|
| $C_{11}^d$ | $0.12348 - 0.02266j$ | $0.00007 - 0.03685j$ |
| $C_{12}^d$ | $-0.01977 + 0.02825j$ | $-0.02563 - 0.02567j$ |
| $C_{13}^d$ | $-0.01220 - 0.06732j$ | $0.03234 + 0.00011j$ |
| $C_{14}^d$ | $-0.00593 + 0.00856j$ | $-0.05535 - 0.05573j$ |
| $C_{15}^d$ | $0.05326 - 0.00974j$ | $0.00011 - 0.04091j$ |
| $C_{16}^d$ | $0.00987 + 0.00652j$ | $0.02545 - 0.02532j$ |

| | $\mathcal{B}(\Gamma_8^{v_2}, \Gamma_8^{v_2})$ | $\mathcal{B}(\Gamma_8^m, \Gamma_8^{v_2})$ |
|---|---|---|
| $C_{11}^d$ | $-0.28674$ | $-0.01600 + 0.11728j$ |
| $C_{12}^d$ | $0.05141 - 0.05145j$ | $-0.01350 - 0.01758j$ |
| $C_{13}^d$ | $0$ | $0.02416 + 0.00324j$ |
| $C_{14}^d$ | $0.00399 - 0.00399j$ | $0.01190 + 0.01558j$ |
| $C_{15}^d$ | $-0.00501$ | $-0.01246 + 0.09213j$ |
| $C_{16}^d$ | $-0.00043 - 0.00053j$ | $0.00590 - 0.00469j$ |

| | $\mathcal{B}(\Gamma_8^c, \Gamma_8^{v_2})$ | $\mathcal{B}(\Gamma_8^m, \Gamma_8^m)$ |
|---|---|---|
| $C_{11}^d$ | $0.02620 + 0.00864j$ | $-0.27831$ |
| $C_{12}^d$ | $0.03349 - 0.01703j$ | $0.11463 - 0.11460j$ |
| $C_{13}^d$ | $0.03764 - 0.11510j$ | $0$ |
| $C_{14}^d$ | $-0.09818 + 0.04980j$ | $-0.00658 + 0.00658j$ |
| $C_{15}^d$ | $0.12014 + 0.03925j$ | $0.21144$ |
| $C_{16}^d$ | $-0.02627 - 0.05172j$ | $-0.00010 - 0.00003j$ |

| | $\mathcal{B}(\Gamma_8^c, \Gamma_8^m)$ | $\mathcal{B}(\Gamma_8^c, \Gamma_8^c)$ |
|---|---|---|
| $C_{11}^d$ | $-0.02085 + 0.11282j$ | $-0.59150$ |
| $C_{12}^d$ | $-0.08063 - 0.11724j$ | $-0.07212 + 0.07314j$ |
| $C_{13}^d$ | $0.28896 + 0.05338j$ | $0$ |
| $C_{14}^d$ | $-0.00592 - 0.00860j$ | $-0.00004 + 0.00004j$ |
| $C_{15}^d$ | $0.01242 - 0.06655j$ | $-0.32318$ |
| $C_{16}^d$ | $0.01612 - 0.01110j$ | $-0.00006 - 0.00004j$ |

## IV. REFERENCES

[1] L. Elcoro, B. Bradlyn, Z. Wang, M. G. Vergniory, J. Cano, C. Felser, B. A. Bernevig, D. Orobengoa, G. de la Flor, and M. I. Aroyo, Double crystallographic groups and their representations on the Bilbao Crystallographic Server, J. Appl. Crystallogr. **50**, 1457 (2017).

[2] M. S. Dresselhaus, G. Dresselhaus, and A. Jorio, *Group Theory: Application to the Physics of Condensed Matter* (Springer-Verlag Berlin Heidelberg, 2008).

[3] L. C. Lew Yan Voon and M. Willatzen, *The k·p Method: Electronic Properties of Semiconductors* (Springer-Verlag Berlin Heidelberg, 2009).

[4] M. H. Weiler, R. L. Aggarwal, and B. Lax, Warping- and inversion-asymmetry-induced cyclotron-harmonic transitions in InSb, Phys. Rev. B **17**, 3269 (1978).